Acta Pharmaceutica Sinica B 2026;16(8):5259−5275

Chinese Pharmaceutical Association
Institute of Materia Medica, Chinese Academy of Medical Sciences

Acta Pharmaceutica Sinica B

www.elsevier.com/locate/apsb
www.sciencedirect.com

ORIGINAL ARTICLE

Targeting SIRT6 epigenetically restrains neutrophil hyperplasia and enhances chemotherapeutic efficacy

Luping Wang[a,b,†], Xiaoqian Wu[a,†], Panxia Wang[a,†], Minshan Zhang[a], Li Li[b], Zhenhan Huang[b], Yang Mao[a], Haoming Chen[c], Qin Wen[d], Wei Liu[b], Zhibin Huang[b], Feifei Li[b], Juan Shen[c,*]

[a]*Guangzhou Municipal and Guangdong Provincial Key Laboratory of Molecular Target & Clinical Pharmacology, The NMPA and State Key Laboratory of Respiratory Disease, School of Pharmaceutical Sciences, Guangzhou Medical University, Guangzhou 511436, China*
[b]*The Innovation Centre of Ministry of Education for Development and Diseases, School of Medicine, South China University of Technology, Guangzhou 510006, China*
[c]*School of Life Sciences and Biopharmaceutics, Guangdong Pharmaceutical University, Guangzhou 510006, China*
[d]*Medical Center of Hematology, Institute of Science Innovation for Blood Ecology and Intelligent Cells, Xinqiao Hospital of Army Medical University, Chongqing 400037, China*

Received 4 June 2025; received in revised form 2 November 2025; accepted 1 December 2025

KEY WORDS

Myeloid malignancy;
Neutrophil hyperplasia;
SIRT6;
Zebrafish;
Chemotherapeutic efficacy;
Histone modification;
Imatinib;
MDL-800

Abstract Myeloproliferative neoplasms (MPNs) are a group of hematologic malignancies for which current treatment options remain limited, underscoring the urgent need to explore novel therapeutic targets and intervention strategies. Through a high-throughput screen of an epigenetic compound library, we identified the SIRT6 allosteric agonist MDL-800 as a potent suppressor of neutrophil hyperplasia. We established an endogenous *sirt6*-mutant zebrafish model that develops a myeloproliferative neoplasm (MPN)-like phenotype, with a 64% incidence in adult zebrafish. Mechanistically, Sirt6 was found to regulate neutrophil proliferation *in vivo* and *in vitro* by deacetylating histone H3K9 at the *c-myb* promoter. Sirt6 deficiency led to aberrant proliferation of neutrophils and hematopoietic stem/progenitor cells, whereas Sirt6 overexpression significantly alleviated neutrophil hyperplasia and MPN-related symptoms. Furthermore, the SIRT6 activator MDL-800 enhanced the efficacy of imatinib and reduced neutrophil proliferation in a zebrafish leukemia model. In xenograft mouse models, the combination of MDL-800 and imatinib significantly inhibited leukemia progression and restored drug sensitivity in imatinib-

*Corresponding author.
E-mail address: shenjuan0412@126.com (Juan Shen).
†These authors made equal contributions to this work.

Peer review under the responsibility of Chinese Pharmaceutical Association and Institute of Materia Medica, Chinese Academy of Medical Sciences.

https://doi.org/10.1016/j.apsb.2026.06.020

resistant cases. This study establishes the Sirt6−c-Myb axis as a core epigenetic pathway for myeloid homeostasis, providing a novel strategy for simultaneously suppressing neutrophil hyperplasia and enhancing chemotherapeutic efficacy in hematologic malignancies.

1. Introduction

Myeloproliferative neoplasms (MPNs) are a group of malignant hematological diseases characterized by abnormal proliferation of one or more blood cell lineages in the bone marrow, frequently associated with therapy resistance[1,2]. Current treatment options for MPNs remain limited, highlighting the need to explore new therapeutic targets and intervention strategies. Although dysregulation of transcription factors is well recognized in myeloid malignancies, the epigenetic mechanisms underlying MPN progression and chemotherapy resistance are not fully understood and warrant further investigation[3-6].

The sirtuin family comprises class III histone deacetylases (HDAC III), which depend on NAD^+ as a cofactor to regulate key biological processes such as metabolism, inflammation and oxidative stress. Among them, SIRT6 is a chromatin binding protein with diverse roles in DNA repair, tumor suppression, and organismal lifespan[7-9]. SIRT6 deacetylates H3K9ac and H3K56ac and acts as a transcriptional corepressor of MYC, PPAR, Wnt, Notch and hypoxia-inducible factor-1α (HIF-1α) signaling pathways[10-14]. Single-cell RNA-Seq has revealed that primitive leukemia cells exhibited dysregulated transcriptional programs with co-expression of myeloid priming genes, which carry prognostic significance[15]. In the hematopoietic system, SIRT6 contributes to the maintenance of hematopoietic stem cell (HSC) homeostasis[12]. Nevertheless, direct evidence linking SIRT6 to MPN pathogenesis-particularly neutrophil hyperplasia-through transcriptional regulation remains lacking.

Aberrant activation or ectopic expression of the proto-oncogene c-MYB has been shown to promote the transformation of hematopoietic progenitors into leukemic cells[16,17]. The c-MYB transcription factor also contributes to chemotherapy resistance either by upregulating oncogenes or downregulating tumor suppressors[18]. It remains unclear whether c-MYB transcription is epigenetically regulated by Sirt6 in neutrophils, and whether such regulation influences neutrophil fate decisions between quiescence and proliferation.

In this study, we found that SIRT6 activator effectively inhibits pathological neutrophil proliferation. We generated an endogenous *sirt6* mutant zebrafish model that recapitulates features of human MPN progression from embryogenesis to adulthood. Mechanistically, SIRT6 directly interacts with the c-Myb promoter region and modulates its transcriptional activity *via* H3K9 deacetylation. Further investigations showed that the SIRT6 activator MDL-800 not only inhibits myeloid expansion but also enhances the efficacy of imatinib.

In summary, this study provides evidence supporting SIRT6 as a potential epigenetic regulator of myeloid homeostasis. Given the current limitations of tyrosine kinase inhibitors (TKI) therapies, our findings suggest that SIRT6 activation may represent a promising therapeutic strategy for MPNs.

2. Materials and methods

2.1. Zebrafish husbandry

All experiments involving zebrafish were performed under approval from the Institutional Animal Care and Use Committee of South China University of Technology. Zebrafish (from fertilization to 2 years old) were maintained as previously reported[19]. The following strains were used in this study: AB (wide type), *pu.1*$^{G242D/G242D}$[,20], *Tg(hsp70:p210*$^{BCR/ABL1}$*)*[21], c-Myb hyperactive (*c-myb*^{hyper})[22], *Tg(cd41*:eGFP)[23] and *Tg(lyz*:DsRed*)*[24].

2.2. Compounds screening

The Epigenetics Compound Library (#L3500, TargetMol, Shanghai, China. Supporting Information Table S1) was utilized. Compounds dissolved in dimethyl sulfoxide (DMSO) (stock concentration: 10 mmol/L) were added in egg water (work concentration: 10 μmol/L) to treat embryos from 24 h post fertilization (hpf) to 3 days post fertilization (dpf) in multi-well plates, the DMSO or compounds-treated embryos were detected by Sudan Black B (SB) (#199664, Sigma−Aldrich, St. Louis, MO, USA) staining at 3 dpf. All compounds were absorbed by zebrafish embryos through immersion.

2.3. SB staining

Fixed embryos subjected to compound treatments as detailed above were incubated in SB solution and performed as previously described[25].

2.4. Generation of sirt6 mutant lines and validation

sirt6 mutants were generated by the CRISPR/Cas9 method. The zebrafish *sirt6* target within exon 2 is 5′-GGATCAGAGAGTCTCAGTACA-3′. *sirt6* guide RNA (gRNA) was transcribed by using mMESSAGE mMACHINE T7 kit (#AM1344, Thermo Fisher Scientific, Waltham, MA, USA). *sirt6* mutants were generated by injecting single-cell stage embryos with Cas9 protein (EnGen Cas9 NLS, NEB, Ipswich, MA, USA) and gRNA. The embryos were raised to adulthood and genetic mutant lines were screened as F_0 founders. F_1 progeny was obtained by crossing F_0 fish with WT fish, then were genotyped and sequenced to identify the inheritable mutation. We obtained the main frameshift mutation with a deletion of 4 bp (F_1). *sirt6*$^{+/+}$ and *sirt6*$^{-/-}$ embryos were generated from heterozygous intercrosses. The genotyping primers of high-resolution melting (HRM) for *sirt6* mutants were listed in Supporting Information Table S2 and Fig. S1.

2.5. Whole mount in situ hybridization (WISH)

The antisense digoxigenin-labeled RNA probes were synthesized based on standard protocols[26]. For WISH, staged embryos were collected and processed with digoxigenin-labeled RNA probes as previously described[27]. WISH signals were counted manually under a stereomicroscope. Each sample was photographed with a different focused Z-plane for representative pictures of WISH.

2.6. Fluorescence activated cell sorting (FACS)

For FACS of *Tg(lyz*:DsRed*);sirt6*$^{+/+}$ and *Tg(lyz*:DsRed*);sirt6*$^{-/-}$ whole embyros. The embryos were collected with a filter with 100 μm pore size, washed and resuspended in phosphate buffered saline (PBS) containing 5% fetal bovine serum (FBS), digested, and then passed through a filter with 40-μm pore size. Flow cytometry analysis and sorting were based on forward scatter and side scatter with a MoFlo AstriosEQ sorter (Beckman Coulter, California, USA).

For FACS of *Tg(lyz*:DsRed*);sirt6*$^{+/+}$ and *Tg(lyz*:DsRed*);sirt6*$^{-/-}$ adult fish kidney marrow (KM). The fish were dissected as described[28] and the KM was removed and placed in PBS containing 5% FBS, and then passed through a filter with 40-μm pore size, the single-cell suspensions were sorted with a MoFlo AstriosEQ sorter. The sorted DsRed^{+} cells were collected in PBS with 5% FBS for other uses.

2.7. RNA extraction and reverse transcription-quantitative polymerase chain reaction (qPCR)

RNA was extracted with TRIzol (Invitrogen, Waltham, MA, USA) and reverse transcribed by M-MLV Reverse Transcriptase (Promega, Madison, WI, USA). The qPCR was conducted using LightCycler 96 instrument (Hoffmann-La Roche Ltd., Basel, Switzerland), the relative gene expression was calculated with the $2^{-\Delta\Delta Ct}$ method, zebrafish elongation factor 1α (*ef1*α) was considered as an internal control. All primers are listed in Table S2.

2.8. Western blotting

Deyolked zebrafish embryos, K562, THP-1, HL-60 or HEK293T cell pellets were homogenized with RIPA Lysis Buffer (#P0013C, Beyotime, Shanghai, China). Western blotting was done according to standard protocols[29]. The antibodies used were as follows: H3K9ac (Novus Biologicals, NBP2-59180, 1:1000), H3K56ac (Novus Biologicals, NBP2-61537, 1:1000), Histone3 (Abcam, ab1791, 1:1000), SIRT6 (Abcam, ab191385, 1:2000), c-MYB (Novus Biologicals, AF6209, 1:1000), ß-actin (Proteintech, 20536-1-AP, 1:5000) and α-tubulin (Proteintech, 11224-1-AP, 1:2000). Detection was with anti-rabbit HRP-conjugated secondary antibodies (Abcam, ab6721, 1:3000, respectively) and SuperSignal West Pico PLUS chemiluminescent substrate (#34577, Thermo Scientific, Waltham, MA, USA).

2.9. May−Grünwald−Giemsa staining

Zebrafish were placed on ice for anesthesia. Peripheral blood (PB) and KM were removed and placed in PBS with 5% FBS. After filtration and Cytospin at 400 rpm (Shandon Cytospin 4, Thermo Scientific, Waltham, MA, USA) for 3 min, the cells were stained with diluted Giemsa (Merck, Darmstadt, Germany) and May−-Grunwald's eosin methylene blue (Merck, Darmstadt, Germany). Blood cells of PB and KM were manually counted and classified according to their morphologies.

2.10. Histological section of zebrafish tissues

Adult zebrafish were fixed in 4% polyformaldehyde (PFA) at least 3 days at 4 °C, following with 20% EDTA (PH = 8.0) about 7 days to decalcify, then dehydrated by ethanol, cleared by xylene, and embedded in paraffin. The zebrafish tissues (including kidney and liver) were sectioned at 5 μm and stained with indicated antibodies or hematoxylin and eosin (HE). For frozen sections, after being fixed by 4% PFA, the fish tissues were deposited in 30% sucrose solution overnight at 4 °C. After precipitation, the tissues were embedded with OCT embedding agent (#4583, Sakura, Torrance, CA, USA) and followed by frozen. Then they were placed into the pre-frozen freezing microtome (Leica, Wetzlar, Germany) for slicing. The frozen sections were stained with the indicated antibodies for immunofluorescence.

2.11. Cell proliferation assay

Tg(lyz:DsRed*);sirt6*$^{+/+}$, *Tg(lyz*:DsRed*);sirt6*$^{-/-}$, *Tg(cd41*:eGFP*);sirt6*$^{+/+}$ and *Tg(cd41*:eGFP*);sirt6*$^{-/-}$ embryos at 3 dpf were incubated in egg water with 10 mmol/L BrdU (Merck, Darmstadt, Germany) for 2 h, then labeled as previously described[30]. *Tg(lyz*:DsRed*);sirt6*$^{+/+}$and *Tg(lyz*:DsRed*);sirt6*$^{-/-}$ zebrafish at 1-year old were incubated with 10 mmol/L BrdU for 4 h, followed by frozen slicing, then labeled as previously described[30]. The following antibodies were used: rabbit-anti-DsRed (Santa Cruz, sc-390909; 1:50), goat anti-GFP (Abcam, ab6658; 1:400), mouse-anti-pH3 (Santa Cruz, sc-374669; 1:50), rabbit-anti-Lcp1 antibody (gift from Dr. Zilong Wen)[31], mouse anti-BrdU (Roche, 11170376001; 1:50), Alexa Fluor 555-conjugated anti-rabbit (Invitrogen, A32732; 1:400) and Alexa Fluor 488-conjugated anti-mouse (Invitrogen, A32723; 1:400).

2.12. Synthesis of sirt6 mRNA

The *sirt6* coding sequence was amplified using primers (5′-ATGTCGGTGAATTACGCCGC-3′ and 5′-TCAAGTGTGTGTGTGTACGTGAG-3′), and the PCR product was inserted into the pCS2^{+} vector. After linearization by Not1, the capped *sirt6* mRNA was synthesized *in vitro* by using an mMESSAGE mMACHINE® SP6 Kit (#AM1340, Thermo Fisher Scientific, Waltham, MA, USA) according to the manufacturer's instructions. The mRNA was injected into each embryo at a concentration of 200 pg.

2.13. Plasmids

For the construction of *pTAL-ef1a-sirt6-DsRed*, *sirt6* cDNA containing the coding region was cloned downstream of *ef1a* promoter. For overexpression of *sirt6*, 1-cell-stage embryos were injected with the DNA construct.

2.14. Morpholino oligonucleotides (MO) injection

A previously described MO for *c-myb* (sequence 5′-tcgccatcccgctgttcgagaggaa-3′, complementary to the translational initiation site; underlined) was purchased from Gene Tools (Philomath, OR, USA) as described[32]. The MO for *c-myb* was injected into zebrafish embryos at one-cell stage at 0.5 mmol/L.

2.15. RNA-sequencing (RNA-seq) data analysis

Embryos were collected at 3 dpf, then grouped into *sirt6/c-myb-hyper/pu.1*$^{G242D/G242D}$ and WT groups through genotyping, total RNA was extracted from the tails including hematopoietic tissue. Each sample library was from around 25 tails. The poly-A selected RNA was applied to the NGS RNA Library Prep kits (Novogene, Beijing, China) to construct Sequencing libraries. The generated fastq files were subjected to FastQC to check sequencing quality. The clean reads were mapped onto the GRCz11 zebrafish reference genome using HISAT2 (v2.0.5)[33]. The mapped reads were then counted using FeatureCounts[34]. The counts matrix was applied to DESeq2 for normalization[35], differentially expressed genes identification. Corrected *P* value of 0.05 and absolute foldchange of 1.5 were set as the threshold for significantly differential expression. The sample-to-sample gene expression heatmap was performed using the TBtools software[36].

2.16. Chromatin immunoprecipitation (ChIP) assay

For Sirt6 ChIP in zebrafish embyros, Myc-Sirt6 plasmid was injected into zebrafish embyros for ChIP assay with Myc antibody or IgG control. For H3K9ac ChIP in zebrafish embyros, about 200 embryos for each group were collected and fixed with 1% formaldehyde at 3 dpf for ChIP assay. The antibodies used for the ChIP assay were as follows: anti-Myc tag (Proteintech, 16286-1-AP), anti-H3K9ac (Novus Biologicals, NBP2-59180), anti-normal rabbit IgG (Cell Signaling Technology, 2729). The ChIP assay was performed as described[37]. Cross-linked samples were sonicated by Covaris M220 sonicator to a size range of 200−600 bp. Then sonicated chromatin samples were immunoprecipitated with indicated antibody (5 μg) and Dynal Protein G magnetic beads. DNA was purified with GeneJET PCR purification kit (Thermo Scientific, K0702). For ChIP-qPCR, analysis was performed with the FastStart SYBR Green Master (Roche). The primers are listed in Table S2.

For H3K9ac ChIP in HEK 293T cells, ChIP was performed according to the manufacturers' instructions by using Magna ChIP HiSens Kit (#17-10460, Merck, Darmstadt, Germany). Chromatin samples were immunoprecipitated with antibodies against H3K9ac (Novus Biologicals, NBP2-59180), and normal rabbit IgG (Cell Signaling Technology, 2729). For ChIP-qPCR, analysis was performed with the FastStart SYBR Green Master (Roche). The primers are listed in Table S2.

2.17. ChIP-sequencing (ChIP-seq) data analysis

For SIRT6 ChIP in K562 cell, ChIP was performed according to the manufacturers' instructions by using Magna ChIP HiSens Kit (#17-10460, Sigma−Aldrich). K562 cells were cross-linked with 1% formaldehyde to fix protein−DNA interactions. After cell lysis, chromatin was fragmented into sizes of 200−500 bp using sonication. The sheared chromatin was then subjected to immunoprecipitation overnight using anti-SIRT6 (Novus Biologicals, NBP3-10936) antibody. A corresponding input DNA sample was collected and processed in parallel to serve as control. Strict wash steps were applied to remove non-specifically bound chromatin, and the protein−DNA cross-links were subsequently reversed. The immunoprecipitated DNA and Input DNA were then purified. Libraries were prepared using the NEB Next Ultra II DNA Library Prep Kit for Illumina and sequenced with PE150 strategy on the Illumina NovaSeq6000 sequencer.

The data analysis was carried out as previously described[38]. Using Burrows−Wheeler Aligner software (v0.1.17)[39], we mapped the sequencing reads to Ensembl Human reference genome (GRCh38). We used the bamCoverage in deepTools[40] (v3.5.1) to visualize the reads in Integrative genomics viewer (IGV). Gene annotation and genomic distribution of these peaks were performed using ChIPseeker[41]. The annotated nearest genes that were 5000 bp upstream to 5000 bp downstream from the transcriptional start site (TSS) were obtained.

2.18. Cell culture and transfections

K562, THP-1, HL-60 and HEK293T cells were maintained in DMEM medium supplemented with 10% FBS in a 37 °C humidified incubator with 5% CO_2 environment. Transient transfections in HEK293T cells were performed using Lipofectamine 3000 (L3000075, Thermo Fisher Scientific, Waltham, MA, USA) following the manufacturer's instructions. Human SIRT6 small interfering RNA target sequences are listed in Table S2.

2.19. Treatment with chemotherapeutic agents in zebrafish

Embryos at 24 hpf were incubated in egg water containing 1‰ DMSO, MDL-800 (Sigma−Aldrich, SML2529, 4 μmol/L), imatinib (Selleck, STI571, 20 μmol/L) respectively, or combination of imatinib (20 μmol/L) with MDL-800 (4 μmol/L). Drugs were absorbed by immersion for zebrafish larvae, the water and drugs were reintroduced at the 3 dpf for 4 days of drug treatment (drugs were added at 24 hpf, and the effects were detected at 5 dpf), Adult fish was intraperitoneally injected with imatinib (2000 mg/kg/day), MDL-800 (1600 mg/kg/day) once daily for 7 days.

2.20. Mouse experiments

The animal experiments were approved by the Animal Research Committee, Guangzhou Medical University (approval number GY2024-056). All the experimental procedures were carried out according to the guidelines for the Care and Use of Laboratory Animals published by the United States National Institutes of Health (NIH Publication, revised 2011). Male NOD-SCID mice (4 weeks old) were obtained from GemPharmatech Co., Ltd., Jiangsu, China. The animal licence number was SCXK (YUE) 2020-0054. All the mice were raised in humidity- and temperature-controlled environment with a 12-h light/dark cycle, with food and water *ad libitum*. The CML model was generated as follows:

For transplantation of K562-GFP cells (including imatinib-sensitive and resistant K562 cell line), 1×10^7 K562-GFP cells were tail vein injected into single half-lethally irradiated (2.0 Gy) NOD-SCID recipient mouse. Mice were orally given MDL-800 (50 mg/kg, TargetMol, T64529) or/and imatinib (100 mg/kg, TargetMol, T6230) for 8 weeks after transplantation. The treatment was repeated daily for the specified duration.

For imatinib-sensitive K562 cell transplantation, a total of 100 mice were randomized into 5 groups: (I) Con + Vehicle, (II) CML + Vehicle, (III) CML + MDL-800, (IV) CML + Imatinib, (V) CML + Imatinib + MDL-800. For imatinib-resistant K562 cell transplantation, a total of 36 mice were randomized into 3 groups: (I) Con + Vehicle, (II) CML + Vehicle, (III) CML + Imatinib + MDL-800. After 8 weeks of gavage administration, peripheral blood was collected by tail vein. Subsequently, the mice were euthanized by carbon dioxide for 2 min from a compressed gas tank followed by cervical dislocation, the femur and tibia were

harvested, and bone marrow cells are flushed out with PBS by 1 mL syringe, peripheral blood and bone marrow blood smear were prepared and stained by May−Grünwald−Giemsa method. The entire spleen and liver tissue of the mice were collected and fixed with a 4% paraformaldehyde solution for further experiments. The fixed tissue was embedded in paraffin and cut into 5 μm thickness for HE staining and immunostaining. The following antibodies were used: goat anti-GFP (Abcam, ab6658; 1:400), mouse anti-PCNA (Abcam, ab29; 1:400), Alexa Fluor 488-conjugated anti-goat (Invitrogen, A32814; 1:400), Alexa Fluor 555-conjugated anti-mouse (Invitrogen, A31570; 1:400).

2.21. *Human specimens*

This study was approved by the Ethics Committee of the Second Affiliated Hospital of Army Medical University (Xinqiao Hospital). All bone marrow samples were collected at the Hematology Medical Center of the same institution between February 2024 and June 2025. The samples included specimens from patients with newly diagnosed CML or acute myeloid leukemia (AML), as well as from healthy donors for hematopoietic stem cell transplantation. The study was registered with the Chinese Clinical Trial Registry under approval numbers ChiCTR-2300075668 and ChiCTR-1800018662.

2.22. *Statistical analysis*

All data were statistically analyzed by GraphPad Prism (version 8.3.0) software. Two-tailed Student's *t* tests were used to determine statistically significant differences between two groups. One-way ANOVA or two-way ANOVA (Fisher's LSD test) was used for multiple comparisons. The log-rank test was used to analyze the survival rate. Data are presented as mean ± standard deviation (SD). Each experiment was independently repeated at least three times. The density of the Western blot bands was analyzed by ImageJ software. Differences were considered significant when P values were <0.05.

3. Results

3.1. *SIRT6 agonist MDL-800 was screened and identified to mitigate neutrophil hyperplasia*

To identify compounds capable of ameliorating the neutrophil expansion phenotype in zebrafish models of neutrophil hyperplasia, we conducted a screen using an epigenetic compound library containing 569 compounds (Table S1). Neutrophils were quantified through SB staining (Fig. 1A). The screen yielded four consistent hits. We identified Entinostat (a class I HDAC selective inhibitor; Supporting Information Fig. S2A), Citarinostat (a class IIb HDAC selective inhibitor; Fig. S2B), and Vorinostat (a pan-inhibitor of class I/II/IV HDAC; Fig. S2C), all of which significantly reduced the proportion of SB^+ neutrophils, indicating alleviation of the neutrophilic expansion phenotype. Strikingly, MDL-800, a SIRT6 (class III HDAC) agonist, was identified as exerting a protective effect, reducing SB^+ cells in three independent neutrophil hyperplasia zebrafish models: *c-myb*^{hyper}, *pu.1*$^{G242D/G242D}$ and *Tg(hsp70:p210*$^{BCR/ABL1}$*)* lines (Fig. 1B−D). Consistently, MDL-800 also reduced *lyz*$^+$ neutrophils in *Tg(lyz:DsRed);c-myb*^{hyper} zebrafish line (Fig. 1E). Conversely, SIRT6 inhibitor OSS-128167 presented aggravating effect with increased SB^+ neutrophils (Supporting Information Fig. S3). Furthermore, MDL-800 treatment inhibited both cell growth (Fig. 1F) and proliferation (Fig. 1G) in K562 leukemia cells *in vitro*. Collectively, these *in vivo* and *in vitro* results indicate that pharmacological activation of SIRT6 significantly mitigates neutrophil hyperplasia.

To examine the spatial expression of *sirt6* in zebrafish, we performed WISH on larvae, which revealed a broad but non-uniform distribution, not confined to any specific tissue (Supporting Information Fig. S4A). In adults, we analyzed a public 10 × single-cell RNA-seq dataset (GEO: GSE206979) from kidney marrow-the zebrafish equivalent of mammalian bone marrow. UMAP visualization identified nine major blood cell populations (Fig. S4B), among which *sirt6* expression was notably higher in myeloid cells, particularly neutrophils and lymphocytes, compared with other lineages (Fig. S4C).

Phylogenetic analysis indicated that zebrafish Sirt6 is evolutionarily conserved among vertebrates (Supporting Information Fig. S5A). Multiple sequence alignment revealed strong conservation in the N-terminal region[42,43], including key catalytic residues (S56, R65, H133, C144) that are essential for SIRT6's deacetylase activity[43-45] (Fig. S5B).

To evaluate the disease relevance of SIRT6 activation, we analyzed clinical bone marrow samples and observed significant downregulation of SIRT6 in CML, but upregulation in AML compared with normal controls (Supporting Information Fig. S6A and S6B). Consistent with this, SIRT6 expression was lower in the CML cell line K562 than in AML lines (THP-1 and HL60) (Fig. S6C and S6D). These consistent findings highlight a specific suppression of SIRT6 in CML and indicate that its activation represents a promising therapeutic strategy for this disease.

3.2. *sirt6 deficiency results in neutrophils expansion in zebrafish at embryonic stage and MPN-like syndrome in adulthood*

To further investigate SIRT6 function in myeloid malignancies, we generated a *sirt6* mutant zebrafish line using the CRISPR/Cas9 system. We obtained an allele with a 4-bp deletion in exon 2 (Supporting Information Fig. S7A). The deletion is predicted to induce a premature stop codon at amino acid 92. qPCR validation confirmed that the mutant produced only the truncated mRNA transcript (Fig. S7B and S7C), consistent with a predicted loss-of-function allele (*sirt6*$^{-/-}$).

We firstly analyzed the impact of Sirt6 deletion on hematopoietic lineages in zebrafish using lineage-specific markers. Primitive hematopoiesis (assessed at ≤24 hpf) remained largely unaffected in *sirt6*$^{-/-}$ mutants, with no significant changes in *gata1*$^+$ erythroid cells, *pu.1*$^+$ common myeloid progenitor cells, *lyz*$^+$*/mpx*$^+$ neutrophils, or *mfap4*$^+$ macrophages (Supporting Information Fig. S8A). However, in definitive hematopoiesis, enhanced output of neutrophils (*lyz*$^+$ and *npsn*$^+$) was found in *sirt6*$^{-/-}$ larvae (Fig. 2A and B). Loss of *sirt6* specifically reduced *mfap4*$^+$ macrophages, while *rag1*$^+$ lymphocytes and *βe1*$^+$ erythrocytes remained unchanged compared to the WT controls (Fig. S8B). Furthermore, *sirt6*$^{-/-}$*;cd41*:eGFP$^+$ cells (a HSPC marker) were significantly increased in the caudal hematopoietic tissue (CHT) region compared to *sirt6*$^{+/+}$*;cd41*:eGFP$^+$ cells (Supporting Information Fig. S9A and S9B). This observation aligns with reported HSPC expansion following SIRT6 deletion in mice[12]. Reconstitution of *sirt6* attenuated neutrophils expansion induced by *sirt6* mutation (Supporting Information Fig. S10A and

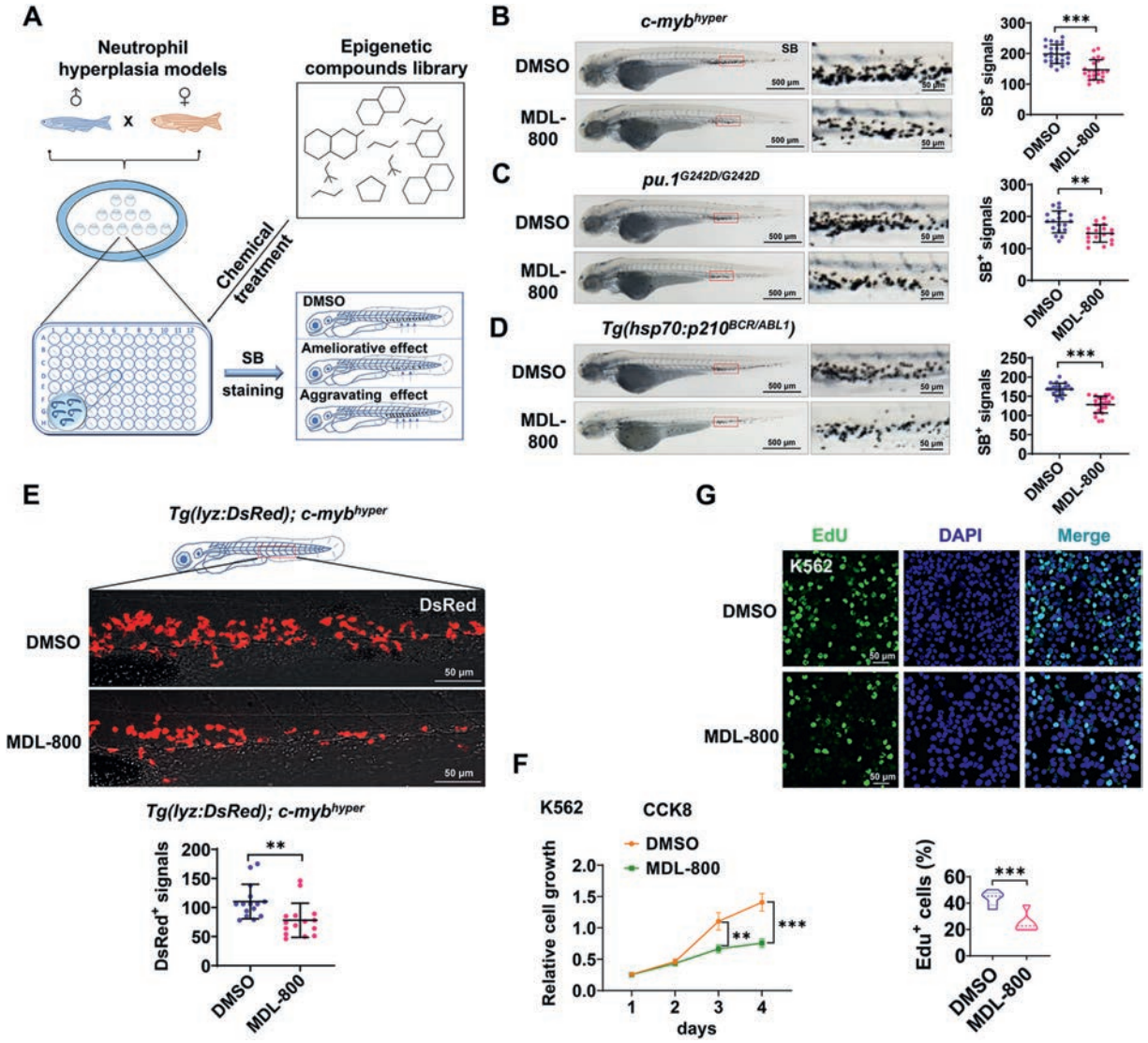

Figure 1 SIRT6 agonist MDL-800 was screened and identified to mitigate neutrophil hyperplasia. (A) Flow diagram of compound screening in zebrafish neutrophil hyperplasia models. Embryos were collected and arrayed in 96-well plates at 24 hpf (hours post fertilization). Each well contained compounds at 10 μmol/L in DMSO and embryo medium. Screening was conducted *via* Sudan Black B (SB) staining at 3 dpf (days post fertilization). Many pairs of zebrafish parents were selected, and the embryos from each parent pair were randomly divided into two groups, one for a compound-treated group and the other for its control (DMSO group). (B−D) MDL-800 was screened and showed alleviated phenotype illustrated by the decreased SB^+ neutrophil cells in *c-myb*^{hyper} (B), *pu.1*$^{G242D/G242D}$ (C), and *Tg(hsp70:p210*$^{BCR/ABL1}$*)* (D) zebrafish neutrophil hyperplasia models. ($n > 20$ larvae per group). (E) The number of $DsRed^+$ neutrophils was detected by fluorescent imaging in *Tg(lyz:DsRed*$^+$*); c-myb*^{hyper} zebrafish ($n = 15$ larvae per group). (F) The growth of K562 cells was measured by CCK8 assay with MDL-800 or DMSO treatment ($n = 4$). (G) EdU staining was conducted to detect the proliferation of K562 cells with or without MDL-800 treatment ($n = 6$). Data are presented as mean ± SD. $^{**}P < 0.01$, $^{***}P < 0.001$.

S10B). Together, *sirt6* deficiency results in HSPCs and neutrophils lineage expansion in zebrafish at embryonic stage.

We next observed that adult *sirt6* mutant zebrafish exhibited pathological features resembling myeloproliferative neoplasms (MPNs), characterized by abnormal neutrophil proliferation. Cytological analysis of PB revealed intermingled granulocytes and blasts in approximately 64% (43/67) of 18-month-old *sirt6*$^{-/-}$ zebrafish (Supporting Information Table S3 and Fig. 2C), a finding rarely seen in the WT controls. Approximately 46% *sirt6*$^{-/-}$ zebrafish exhibited an increased proportion of myeloid cells (primarily neutrophils) in PB and kidney marrow (KM, which resembles human bone marrow), with blasts accounting for <10% of the KM (we defined: MPN-Phase1) (Fig. 2D−F). In the late phase, hemocyte differentiation was disrupted, and 12% *sirt6*$^{-/-}$ zebrafish showed increased blasts accounting for >10% and <20% in KM (MPN-Phase2) (Fig. 2D−F). Lastly, 6% *sirt6*$^{-/-}$ zebrafish developed to a severe stage characterized by blasts expanding to >20% in KM (MPN-Phase3) (Fig. 2D−F). Consistent with the MPN-like syndrome observed in *sirt6*$^{-/-}$ zebrafish, the mutants exhibited significant hepatomegaly (Supporting Information Fig. S11A and S11B). Histological examination of livers in MPN-like *sirt6*$^{-/-}$ zebrafish revealed pathological changes, including massive fat vacuoles, narrow hepatic sinusoids, perivascular macrophages infiltration and neutrophils exudation

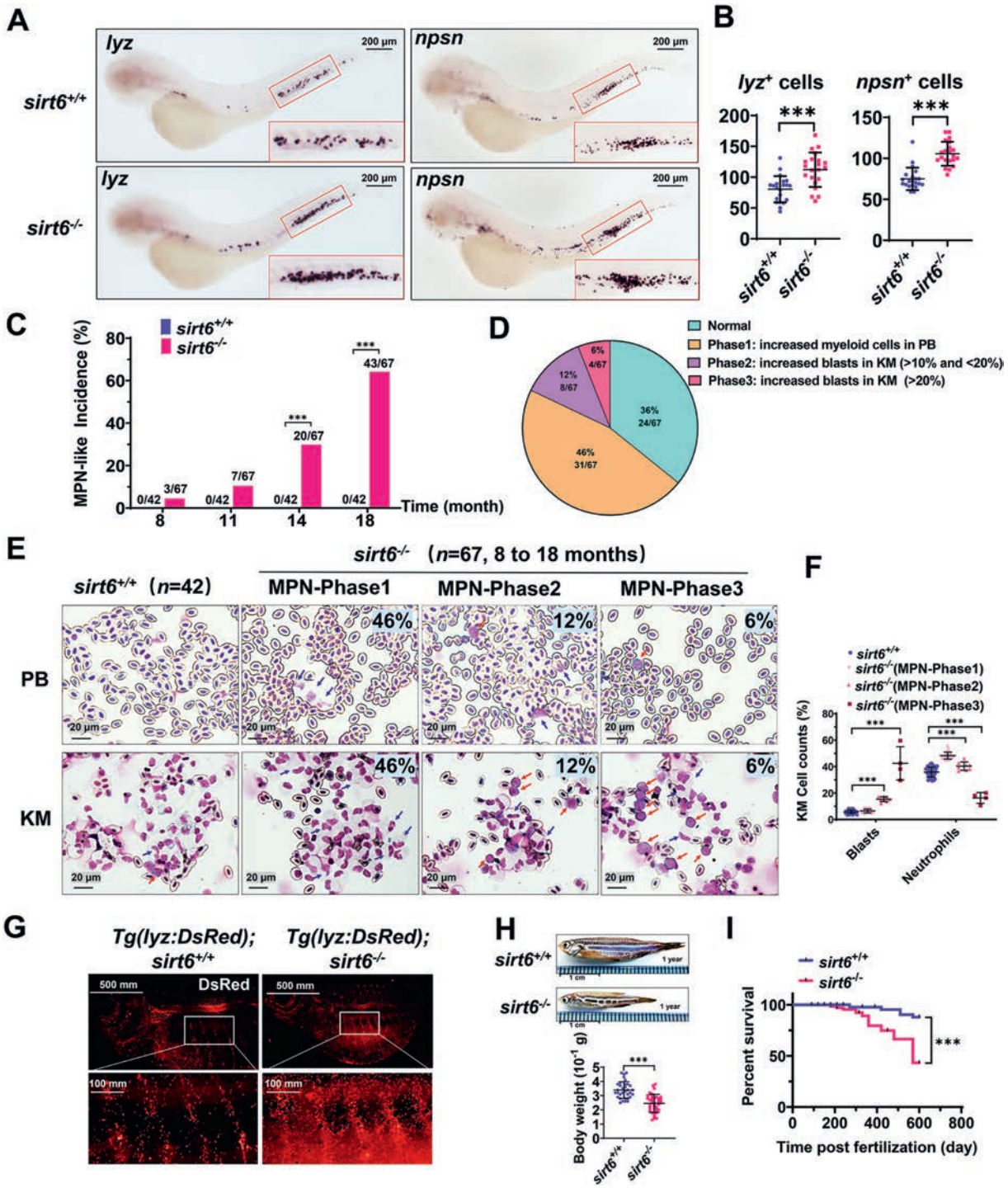

Figure 2 *sirt6* deficiency results in neutrophil expansion in zebrafish at the embryonic stage and MPN-like syndrome in adulthood. (A, B) Whole mount *in situ* hybridization (WISH) of *lyz*, *npsn* expression at 3 dpf in *sirt6*$^{+/+}$ and *sirt6*$^{-/-}$ zebrafish. The caudal hematopoietic tissue (CHT) of zebrafish is enlarged in the red box ($n > 20$ larvae per group). (C, D) The total incidence of MPN (C) and the different phases of MPN (D) in *sirt6*$^{-/-}$ adult zebrafish aged from 4 to 18 months was calculated. (E) May−Grünwald−Giemsa staining of peripheral blood (PB) cells and kidney marrow (KM) cells were obtained from *sirt6*$^{+/+}$ ($n = 42$) and *sirt6*$^{-/-}$ ($n = 67$) adult zebrafish. (red arrows indicate blasts; blue arrows indicate neutrophils). The percentages showed the ratio of fish with indicated MPN-like phase in *sirt6*$^{-/-}$ adult zebrafish. (F) Blood cell counts of KM from *sirt6*$^{+/+}$ and *sirt6*$^{-/-}$adult zebrafish were calculated manually based on their morphology. (G) Fluorescent images present the dispersive degree of *lyz*:DsRed^{+} cells over the body surface. (H) Gross appearance and body weight of *sirt6*$^{-/-}$zebrafish compared with the littermates (1 year old). (I) Survival curve of *sirt6*$^{-/-}$ mutants and siblings was calculated. Data are presented as mean ± SD. ***$P < 0.001$.

(Fig. S11C). These findings are analogous to nonalcoholic fatty liver disease (NAFLD) where macrophages and neutrophils play pivotal roles[46]. In addition, widespread dispersion of DsRed^{+} neutrophils was more easily detected in *Tg(lyz:DsRed^{+}); sirt6$^{-/-}$* mutants compared to the WT group (Fig. 2G). Finally, most surviving *sirt6$^{-/-}$* mutants displayed lower body weight, intermittent skin streaking, and a generally aged appearance (Fig. 2H), contributing to a significantly reduced survival rate after one year of age (Fig. 2I). Collectively, the hematological pathological phenotypes and organ infiltrations in *sirt6$^{-/-}$* mutants closely resembled MPN-like symptoms.

3.3. *sirt6 deficiency drives aberrant hyperproliferation of neutrophils and HSPCs*

To investigate how *sirt6* deficiency drives neutrophil expansion, we performed RNA-sequencing of *sirt6* mutants and its littermate controls. Data analysis (Supporting Information Table S4, and GSE227668) revealed that the cell division pathway was significantly enriched by Gene Ontology (GO) analysis (Fig. 3A). Specifically, genes promoting cell cycle including *cdk4*, *cdk8*, *cdk11b*, *cdk12*, *cdk13* and *ccna2*, were upregulated in *sirt6$^{-/-}$* mutants (Fig. 3B), while the cell cycle inhibiting gene *cdkn1d* was

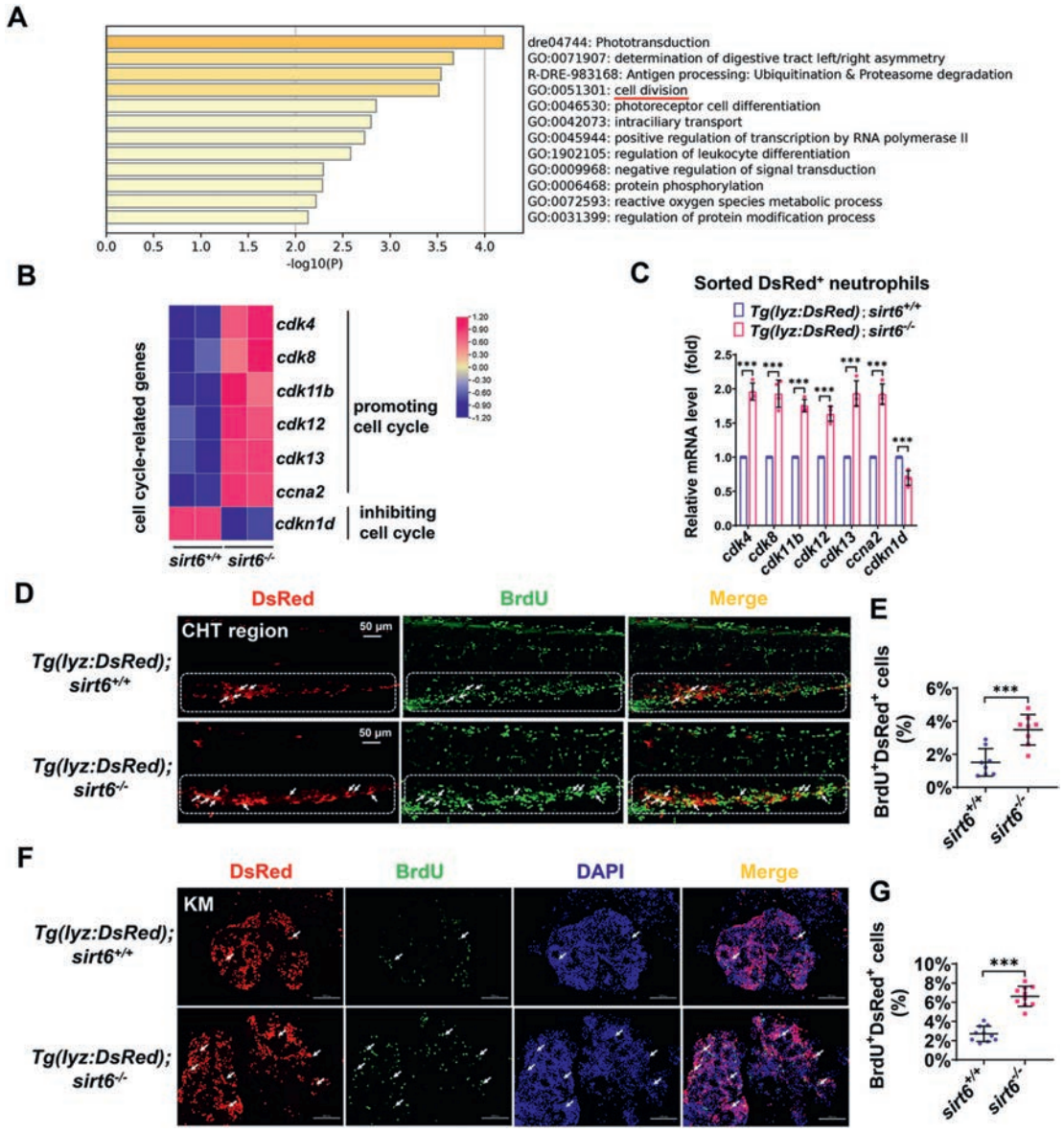

Figure 3 *sirt6* is a neoplastic suppressor that restricts cell cycle and proliferation. (A) Gene ontology (GO) enrichment analysis of biological processes based on differentially expressed genes identified through RNA-sequencing (hypergeometric test), the cell division pathway is highlighted by the red underline. (B) Heatmap displaying the levels of cell cycle promoting/inhibiting genes. (C) The *lyz*:DsRed^{+} neutrophils from 3 dpf larvae were sorted by FACS and applied to qPCR from *Tg(lyz:DsRed^{+});sirt6$^{+/+}$* and *Tg(lyz:DsRed^{+});sirt6$^{-/-}$* zebrafish ($n = 4$). (D) Double staining of DsRed and BrdU in the CHT region of zebrafish larvae at 3 dpf (white arrows indicate BrdU^{+} DsRed^{+} cells). (E) The percentage of BrdU^{+} DsRed^{+} cells was calculated ($n = 8$ per group). (F) The frozen sections of kidney marrow (KM) from adult zebrafish were doubled stained with DsRed and BrdU (white arrows indicate BrdU^{+} DsRed^{+} cells). (G) The percentage of BrdU^{+} DsRed^{+} cells was calculated ($n = 10$ per group). Data are presented as mean ± SD. ***$P < 0.001$.

downregulated in the mutants (Fig. 3B). These expression changes were confirmed in sorted neutrophils from the KM of *Tg(lyz:DsRed$^+$)* zebrafish (Fig. 3C). Neutrophil proliferation was significantly higher in *sirt6*$^{-/-}$ mutants, as shown by BrdU/DsRed co-staining and immunofluorescence in KM (Fig. 3D−G). Since *lyz* is expressed predominantly in early to intermediate maturation stages of neutrophils in zebrafish[47], during which neutrophils remain proliferative[48], the data suggest that Sirt6 may influence early immature neutrophils proliferation.

Additionally, *sirt6*$^{-/-}$ larvae exhibited increased proliferation (BrdU$^+$ and pH3$^+$) in cd41:eGFP$^+$ HSPCs (Supporting Information Fig. S12A and S12B). Together, these data suggest that *sirt6* loss leads to hyperproliferation of both neutrophils and HSPCs.

3.4. Decreased deacetylation of H3K9 by Sirt6 deficiency upregulates c-myb expression and activation

To further elucidate the underlying molecular mechanisms of *sirt6* deficiency-meditated expansion of neutrophils, we performed RNA-seq of *sirt6* mutants and its littermate controls on 3 dpf (Supporting Information Table S5). Given that the SIRT6 agonist MDL-800 reduced neutrophil hyperplasia in zebrafish models including *c-myb*^{hyper} and *pu.1*$^{G242D/G242D}$ lines as previously demonstrated, we also conducted RNA-seqs on the two lines (Supporting Information Tables S6 and S7). Venn analysis identified nine differentially expressed genes common to all three datasets: *si:ch1073429i10.1*, *myb*, *rom1b*, *srgn*, *ttc28*, *notch1b*, *sms*, *ch25hl2*, and *npsn* (Fig. 4A). Based on the established role of *c-myb* as a leukemogenic driver through promoting neutrophil proliferation[22], this study focused on Sirt6-mediated regulation of *c-myb*. Further, we used two AML clinical studies from cBioPortal to analyze the expression relationship between *SIRT6* and *MYB* (Fig. 4B and C). Results revealed a significant inverse correlation between *MYB* and *SIRT6* expression in 671 AML patients (OHSU, Cancer Cell 2022; Spearman's: P = 6.67e-31, R = −0.43; Pearson's: P = 1.76e-34, R = −0.45) and 162 AML patients (TCGA, NEJM 2013; Spearman's: P = 1.335e-5, R = −0.33; Pearson's: P = 9.906e-5, R = −0.30), suggesting a synergistic role of *MYB* hyperactivation and *SIRT6* deficiency. WISH analysis showed elevated *c-myb* expression in *sirt6*$^{-/-}$ mutants (Fig. 4D and E). Moreover, DsRed$^+$ neutrophils sorted from adult zebrafish kidney marrow exhibited increased *c-myb* mRNA levels in *Tg(lyz:DsRed$^+$);sirt6*$^{-/-}$ mutants compared to controls (Fig. 4F). Flow cytometry analysis revealed a lower proportion of *c-myb* GFP$^+$ cells in *c-myb*^{hyper} embryos treated with MDL-800 versus DMSO (Supporting Information Fig. S13A and S13B). Double staining for endogenous *c-myb* RNA and *cd41*:eGFP showed that most expanded *cd41*:eGFP$^+$ HSPCs were also positive for *c-myb* (Supporting Information Fig. S14A and S14B), indicating that Sirt6 regulates *c-myb* expression in both neutrophils and HSPCs.

We extended these observations to the K562 cell line. MDL-800 significantly decreased *c-MYB* mRNA and protein levels (Supporting Information Fig. S15A and S15B). Conversely, the SIRT6 inhibitor OSS-128167 increased them (Fig. S15C and S15D). An *in vivo* GFP reporter assay using a *c-myb* promoter construct showed that *sirt6* deficiency enhanced *c-myb* transcriptional activity (Fig. 4G−I).

Since SIRT6 deacetylates H3K9 and H3K56 to regulate gene expression by modifying chromatin structure[49,50]. We detected the increased level of H3K9ac but not H3K56ac in *sirt6*$^{-/-}$ mutants (Fig. 4J). Immunohistochemical staining (Fig. 4K) and IF staining (Fig. 4L) also confirmed increased H3K9ac level in KM of *sirt6*$^{-/-}$ zebrafish. To map genome-wide SIRT6 binding, we performed SIRT6 ChIP-seq analysis (Supporting Information Fig. S16A and S16B). SIRT6 was robustly enriched at the *c-MYB* promoter region (Fig. S16C), Published ChIP-seq data further showed that MDL-800 reduced H3K9ac signal at this locus[51] (Fig. S16D). Consistently, ChIP-qPCR confirmed Sirt6 binding and H3K9ac enrichment the *c-myb* promoter under physiological conditions (Fig. 4M−O), indicating that SIRT6 constitutively binds and modulates acetylation to maintain a controlled baseline. *sirt6* deficiency increased H3K9 acetylation of the *c-myb* promoter region (Fig. 4P). Accordingly, *c-myb* downstream target myeloid genes such as *lyz*, *mpx*, *npsn* and *srgn* were upregulated in *sirt6*$^{-/-}$ mutants (Supporting Information Fig. S17A and S17B).

Finally, in HEK 293T cells, knockdown of SIRT6 using two independent siRNAs (Si1 and Si2) (Supporting Information Fig. S18A) increased the level of H3K9ac (Fig. S18B) and enhanced H3K9ac enrichment at the *c-MYB* promoter (Fig. S18C). Collectively, these data demonstrate that Sirt6 binds the *c-myb* promoter and represses its transcription through H3K9 deacetylation.

3.5. c-myb deficiency attenuates neutrophils expansion in sirt6$^{-/-}$ mutants

To determine whether neutrophil hyperplasia induced by Sirt6 deficiency is associated with enhanced *c-myb* activation, we knocked down *c-myb* by injecting specific MOs. The increased number of *lyz*$^+$ and *mpx*$^+$ neutrophils were significantly reversed in *sirt6*$^{-/-}$ larvae following *c-myb* knockdown (Fig. 5A−C). Furthermore, *c-myb* deficiency ameliorated the hyperproliferation of neutrophils in *sirt6*$^{-/-}$ mutants (Fig. 5D and E). We next tested the effect of Flavopiridol, a CDK9 inhibitor widely recognized as a broad-spectrum transcriptional inhibitor reported to reduce *c-myb* expression[22]. After intraperitoneal administration of Flavopiridol (150 mg/kg once daily for 5 days) to *sirt6*$^{-/-}$ mutants, *c-myb* expression was notably decreased (Supporting Information Fig. S19), and the elevated proportions of blasts and neutrophils were reduced (Supporting Information Fig. S20A and S20B). These results indicate that Flavopiridol alleviates the MPN-like phenotype driven by *sirt6* deficiency, likely through inhibition of CDK9-mediated transcription, including that of *c-myb*.

Together, these findings demonstrate that Sirt6 constrains neutrophil hyperplasia/MPN progression through a *c-myb*-dependent mechanism.

3.6. Genetic activation of sirt6 ameliorates neutrophil hyperplasia

To confirm the therapeutic effect of genetically activating *sirt6* on neutrophil hyperplasia/MPN, we generated a transgenic zebrafish line: *Tg(ef1a-sirt6-DsRed)*, for *sirt6* overexpression (*sirt6* OE) under the control of the *ef1a* promoter (Fig. 6A). Successful *sirt6* overexpression was confirmed by strong DsRed fluorescence (Fig. 6A) and markedly increased *sirt6* mRNA (Fig. 6B). Consistently, decreased H3K9ac in *sirt6* OE zebrafish (Supporting Information Fig. S21) confirmed effective genetic activation of Sirt6. Moreover, *sirt6* OE reduced H3K9 acetylation level at the *c-myb* promoter (Supporting Information Fig. S22A) and downregulated *c-myb* mRNA expression (Fig. S22B).

To explore whether *sirt6* genetic activation could ameliorate neutrophils hyperplasia, we outcrossed *sirt6* OE zebrafish with

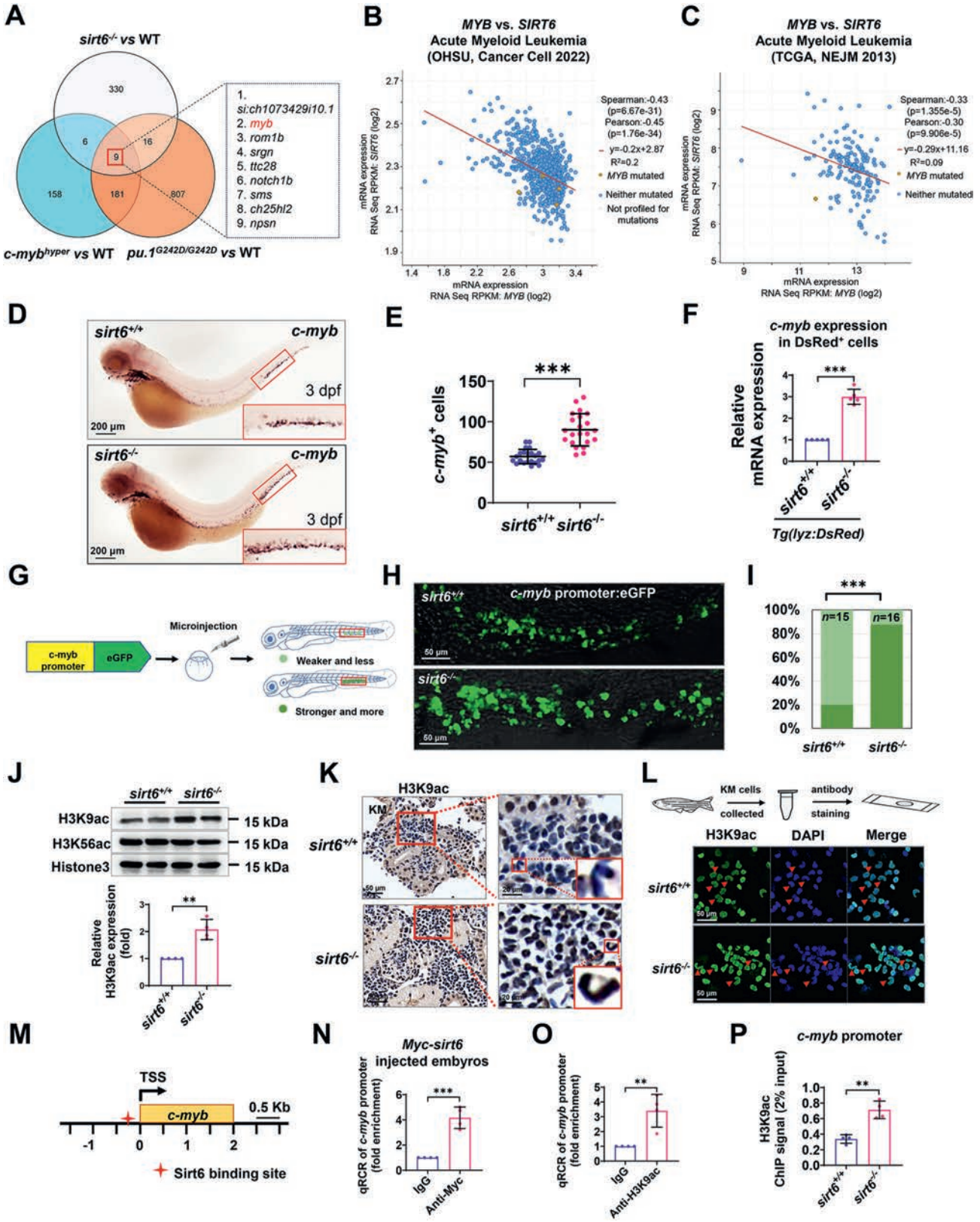

Figure 4 Deacetylation of H3K9 by Sirt6 up-regulates *c-myb* expression and activation. (A) Three RNA-seqs were conducted on *sirt6*$^{-/-}$, *c-myb*^{hyper} and *pu.1*$^{G242D/G242D}$ zebrafish and their littermate controls. A total of 9 genes were intercrossed in the venn plots of these three datasets. (B, C) Results showed an inverse correlation between *MYB* and *SIRT6* expression in 671 AML patients (OHSU, Cancer Cell 2022) (B) and 162 AML patients (TCGA, NEJM 2013) (C). (D, E) WISH of *c-myb* from *sirt6*$^{+/+}$ and *sirt6*$^{-/-}$ zebrafish at 3 dpf ($n > 20$ larvae per group). (F) The *lyz*:DsRed^{+} neutrophils from 3 dpf larvae were sorted by FACS and applied to qPCR ($n = 5$). (G) The procedure of GFP reporter assay.

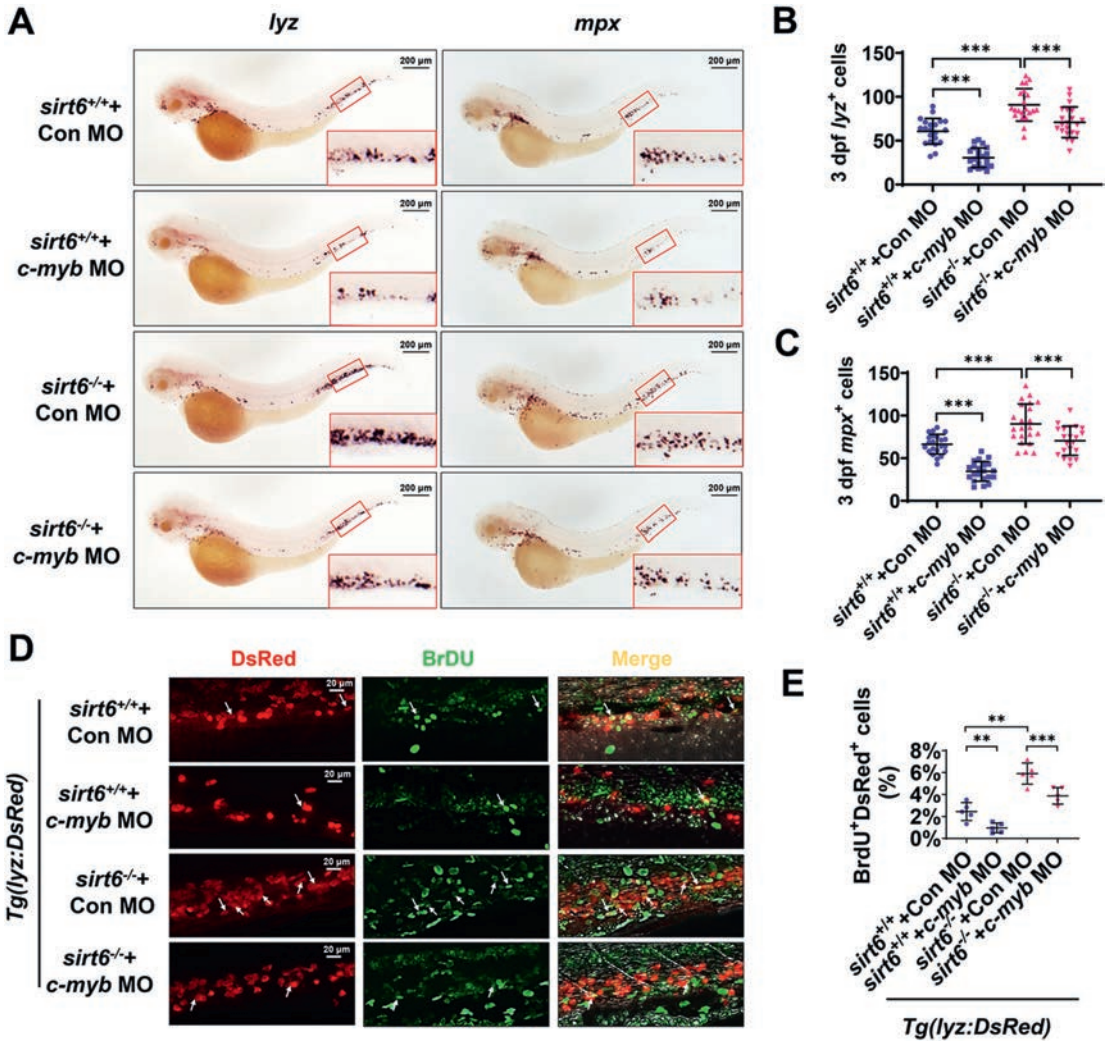

Figure 5 *c-myb* deficiency attenuates neutrophils expansion in *sirt6*$^{-/-}$ mutants. (A–C) WISH of *lyz* and *mpx* of *sirt6*$^{+/+}$ and *sirt6*$^{-/-}$ larvaes with or without injection of *c-myb* Morpholino oligonucleotide (MO) at 3 dpf ($n > 20$ larvae per group). (D, E) Double staining of DsRed and BrdU in the CHT region from *Tg(lyz:DsRed*$^{+}$*);sirt6*$^{+/+}$ and *Tg(lyz:DsRed*$^{+}$*);sirt6*$^{-/-}$ larvaes with or without *c-myb* MO ($n = 5$). Data are presented as mean ± SD. $^{**}P < 0.01$, $^{***}P < 0.001$.

sirt6$^{-/-}$;*c-myb*^{hyper} zebrafish. WISH revealed that *sirt6* overexpression downregulated *c-myb* expression (Fig. 6C) and markedly attenuated the expansion of *lyz*$^{+}$ and *mpx*$^{+}$ neutrophils (Fig. 6C). Additionally, cytological analysis of KM indicated that *sirt6* overexpression decreased the proportions of blasts and neutrophils (Fig. 6D and E). Taken together, these data demonstrate that genetic activation of *sirt6* ameliorates neutrophil hyperplasia and thus corrects associated myeloid abnormalities.

3.7. SIRT6 activator MDL-800 treatment with imatinib improves chemotherapy efficacy

While imatinib has markedly prolonged survival in CML patients, long-term administration frequently leads to therapeutic resistance[52-54]. We therefore evaluated the potential of the SIRT6 activator MDL-800 to enhance imatinib's efficacy through combination therapy in zebrafish and mouse models. We utilized the previously

c-myb-promoter (−5k): eGFP plasmid was injected into one-cell stage embryos. Two groups were classified by GFP fluorescence intensity and the number of GFP + cells. Light green represents weaker GFP expression and fewer GFP^{+} cells. Deep green represents stronger GFP expression and more GFP^{+} cells. (H) Representative *c-myb*-pro: eGFP fluorescence images. (I) The percentage of the indicated group in *sirt6*$^{+/+}$ and *sirt6*$^{-/-}$ larvaes. (J) Western blot of H3K9ac and H3K56ac in the *sirt6*$^{+/+}$ and *sirt6*$^{-/-}$ larvaes at 3 dpf ($n = 4$). (K) The level of H3K9ac was detected in the KM of *sirt6*$^{+/+}$ and *sirt6*$^{-/-}$ adult zebrafish. (L) IF staining of H3K9ac in the KM of *sirt6*$^{+/+}$ and *sirt6*$^{-/-}$ adult zebrafish. (M) Schematic of the *c-myb* promoter. Sirt6 binding on the *c-myb* promoter region is labeled with a red star (−0.5 kb ~ TSS). (N) Myc-Sirt6 plasmid was injected into zebrafish embryos for Chromatin immunoprecipitation (ChIP) assay with Myc antibody or IgG control ($n = 4$). (O) ChIP analysis detected H3K9 acetylation at the promoter of *c-myb* compared with IgG control ($n = 4$). (P) ChIP analysis detected H3K9 acetylation at the promoter of *c-myb* in *sirt6*$^{+/+}$ and *sirt6*$^{-/-}$ zebrafish larvaes ($n = 4$). Data are presented as mean ± SD. $^{**}P < 0.01$, $^{***}P < 0.001$.

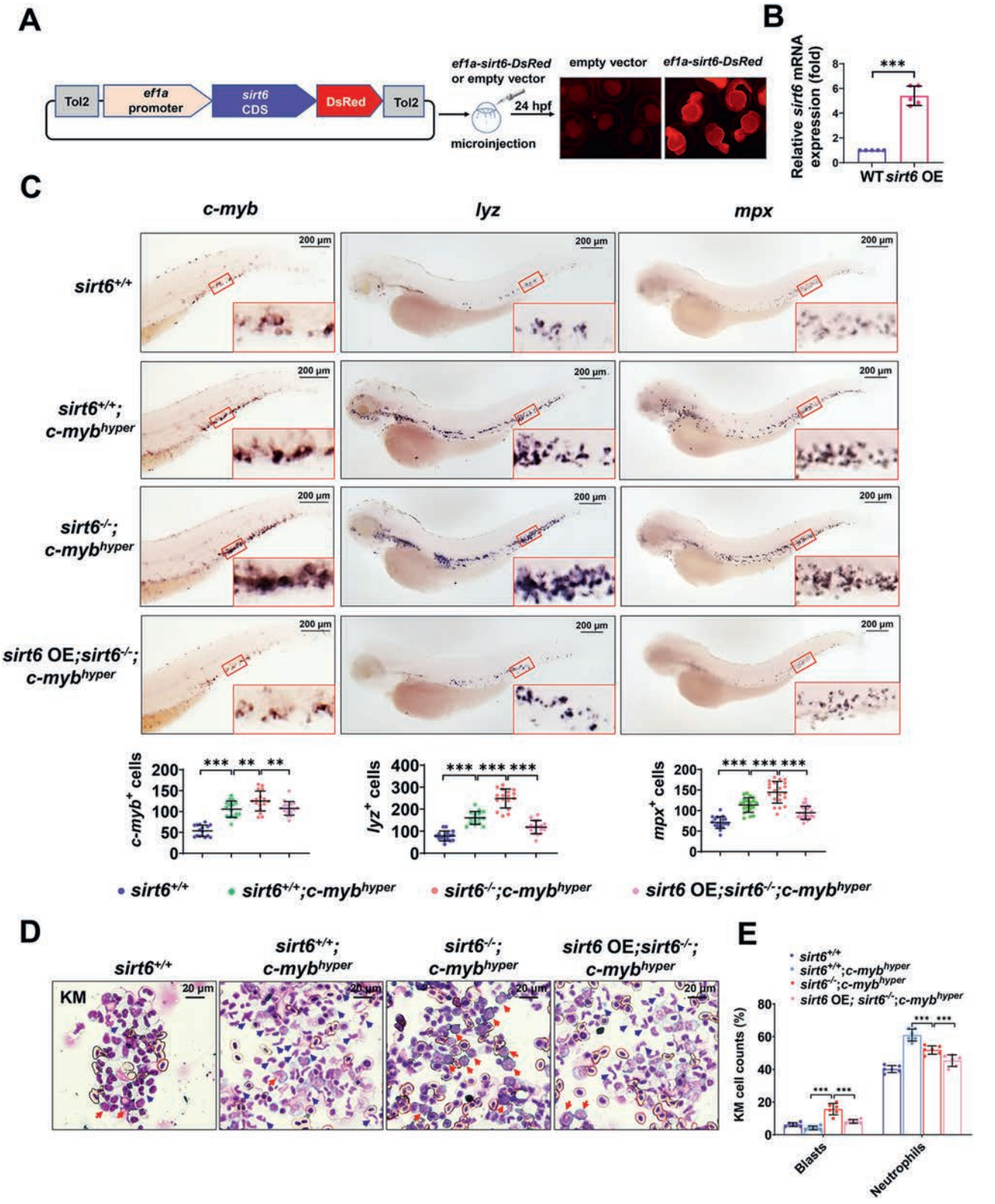

Figure 6 Genetic activation of sirt6 ameliorates neutrophil hyperplasia. (A) The *ef1a* promoter-driven *Tg(ef1a-sirt6-DsRed)* overexpression zebrafish were established. Strong DsRed fluorescence was shown in *Tg(ef1a-sirt6-DsRed)* zebrafish. (B) qPCR showed markedly increased *sirt6* mRNA expression in *Tg(ef1a-sirt6-DsRed)* (*sirt6* OE) zebrafish. *sirt6* OE zebrafish was outcrossed with $sirt6^{-/-}$;$c\text{-}myb^{hyper}$ to generate *sirt6* OE; $sirt6^{-/-}$; $c\text{-}myb^{hyper}$ zebrafish. (C) WISH of *c-myb*, *lyz* and *mpx* at 3 dpf in $sirt6^{+/+}$, $sirt6^{+/+}$; $c\text{-}myb^{hyper}$, $sirt6^{-/-}$; $c\text{-}myb^{hyper}$ and *sirt6* OE; $sirt6^{-/-}$; $c\text{-}myb^{hyper}$ zebrafish. The CHT region is enlarged in the red box ($n > 20$ larvae per group). (D, E) May-Grünwald-Giemsa staining of KM blood cells obtained from $sirt6^{+/+}$, $sirt6^{+/+}$; $c\text{-}myb^{hyper}$, $sirt6^{-/-}$; $c\text{-}myb^{hyper}$, and *sirt6* OE; $sirt6^{-/-}$; $c\text{-}myb^{hyper}$ adult zebrafish (red arrows indicate blasts; blue arrows indicate neutrophils; $n = 6$ larvae per group). Data are presented as mean ± SD. $^{**}P < 0.01$, $^{***}P < 0.001$.

established *Tg(hsp70:p210$^{BCR/ABL1}$);c-myb^{hyper}* zebrafish model of neutrophilia[55]. Four treatment groups were established: DMSO control, MDL-800 alone, imatinib (IMA) alone, and IMA + MDL-800 combination. First, we determined the maximum tolerated concentration of MDL-800 to be 4 μmol/L in zebrafish embryos (Supporting Information Fig. S23A and S23B). Based on our previous report[22], we used IMA at 20 μmol/L, a concentration known to significantly reduce the expanded myeloid population in *Tg(hsp70:p210$^{BCR/ABL1}$)* embryos. For the MDL-800 or IMA groups, embryos were incubated with 4 μmol/L MDL-800 or 20 μmol/L IMA at 1 dpf, and SB$^+$ neutrophils were calculated at 5 dpf (Fig. 7A). The combined administration of 20 μmol/L IMA and 4 μmol/L MDL-800 for 4 days did not cause significant toxicity (Supporting Information Fig. S24). All treatments reduced neutrophil counts, with IMA + MDL-800 combination showing the most significant effect (Fig. 7B and C). Consistently, either MDL-800 or IMA alone decreased the proportion of proliferative myeloid cells (BrdU$^+$/Lcp1$^+$), and the combination treatment was more effective in *Tg(hsp70:p210$^{BCR/ABL1}$);c-myb^{hyper}* larvae (Fig. 7D and E).

Additionally, we further evaluated the efficacy of the drug combination against leukemic granulocytes in adult zebrafish (Fig. 7F). Compared to monotherapy with MDL-800 (1600 mg/kg/day) or IMA (2000 mg/kg/day), the IMA (1600 mg/kg/day) + MDL-800 (2000 mg/kg/day) combination showed better therapeutic effects with more decreased neutrophil proportion in the *Tg(hsp70:p210$^{BCR/ABL1}$);c-myb^{hyper}* model (Fig. 7G and H).

Next, we employed a cell line-derived xenograft (CDX) model by transplanting CML K562-GFP cells into sub-lethally irradiated immunocompromised NOD-SCID mice to assess the synergistic effects of MDL-800 with IMA (Fig. 7I). The transplanted mice developed CML, characterized by increased blast counts in PB and BM (Fig. 7J and K). Cytological analysis revealed that about 70% CML mice treated with IMA alone (100 mg/kg/day) inhibited expansion of blasts (the IMA-effective group). However, the remaining 30% showed no significant response (the IMA-ineffective group) (Fig. 7J and K), indicating the development of chemoresistance or reduced drug sensitivity. Importantly, the IMA (100 mg/kg/day) + MDL-800 (50 mg/kg/day) combination treatment resulted in a marked reduction of blast expansion in all treated mice (Fig. 7J and K, Supporting Information Fig. S25). Furthermore, the combination therapy provided superior protection with more decreased leukemia cells than the IMA-effective group (Fig. 7J and K, Fig. S25). Notably, co-administration of IMA with MDL-800 ameliorated splenomegaly (Fig. 7L), reduced leukemic infiltration in the spleen (Fig. 7L and M, Supporting Information Fig. S26) and liver (Fig. S26), and suppressed elevated *c-Myb* expression (Fig. 7N). The combination treatment also decreased the proportion of proliferative leukemia cells (PCNA$^+$/GFP$^+$) in the spleen (Fig. 7O and P). These data suggest that SIRT6 agonist acts *via* a dual mechanism, simultaneously alleviating neutrophil hyperplasia and enhancing chemotherapeutic efficacy in CML.

To investigate whether MDL-800 could restore IMA sensitivity specifically in a resistant setting, we used an IMA -resistant K562 cell line[56,57]-derived xenograft (CDX) model (IMA-R CML model). As shown in Supporting Information Fig. S27A−S27C, the combination of IMA and MDL-800 significantly decreased blast expansion in treated mice. Co-administration also ameliorated splenomegaly (Fig. S27A), reduced leukemic infiltration in spleen (Fig. S27A and S27D), and inhibited increased *c-Myb* expression (Fig. S27E). Finally, the combination treatment decreased the proportion of proliferative leukemia cells (PCNA$^+$/GFP$^+$) in the spleen (Fig. S27F and S27G). These results demonstrate that MDL-800 could restore sensitivity to IMA.

Importantly, we analyzed SIRT6 and c-MYB expression in bone marrow samples from IMA-R and imatinib-sensitive (IMA-S) groups respectively. A consistent and significant inverse correlation was observed between SIRT6 and c-MYB levels. Specifically, the IMA-R group exhibited markedly decreased SIRT6 expression alongside elevated c-MYB expression at both mRNA and protein levels, compared to the IMA-S group (Supporting Information Fig. S28A−S28E). These data highlight the SIRT6/c-Myb axis as a potential predictive biomarker for IMA treatment response.

4. Discussion

This study reveals Sirt6 as an epigenetic regulator of neutrophil proliferation and myeloid malignancies, offering insights into potential mechanisms and therapeutic strategies. By integrating zebrafish and mouse models with molecular analyses and pharmacological interventions, we demonstrate that Sirt6 deficiency promotes neutrophil hyperplasia and MPN-like phenotypes, whereas Sirt6 activation alleviates these phenotypes—a finding that may provide clues for understanding and treating myeloid disorders.

The transcription factor c-MYB regulates HSPC maintenance and myeloid differentiation, with conserved function across vertebrates[32,58]. Its clinical relevance is underscored by frequent dysregulation through amplification or regulatory mutations in myeloid malignancies like AML/CML[59]. Our team and others have developed zebrafish and mouse models with c-Myb hyperactivation, which closely resemble human leukemia in pathology, disease progression, molecular mechanisms, and drug sensitivity[22,60]. Taking advantage of zebrafish's compact size, optical accessibility and high-throughput potential, we have utilized the *c-myb^{hyper}* line for drug screening, providing unique *in vivo* support for therapeutic strategies against hematological diseases. We previously identified 17β-estradiol (E2) as an anti-neutrophil hyperplasia therapeutic through screening in *c-myb*$^{\text{hyper}}$ zebrafish[61]. Advances in cancer epigenetics have led to the development of promising anti-leukemic agents such as DNA methyltransferase inhibitors and HDAC inhibitors[62]. Acute T-cell leukemia cells which were sensitive to HDAC inhibitor vorinostat-induced cell death also showed MYBL2 downregulation[63]. In the present study, we characterized the anti-neutrophil hyperplasia activity of another hit from epigenetic compound library: the SIRT6 activator MDL-800.

Research on the role of SIRT6 activation in leukemia chemoresistance remains limited. Here, we highlight MDL-800 as a promising therapeutic agent that effectively attenuates MPN/neutrophil hyperplasia in zebrafish and murine models. Notably, MDL-800 synergizes with imatinib, enhancing therapeutic efficacy and improving chemosensitivity. Our results suggest that combination therapy with MDL-800 may benefit certain patients with TKI-resistant CML. The potential target populations could include those harboring BCR-ABL1 kinase domain mutations[64], or exhibiting intrinsic resistance driven by factors such as highly active *c-MYB* in leukemic stem cells[65]—a hypothesis that warrants further investigation.

Strikingly, our findings indicate that the SIRT6/c-MYB axis may serve as a potential predictive biomarker. In CDX models, we observed a consistent pattern of SIRT6 suppression accompanied by c-MYB elevation, which appears to correlate with imatinib

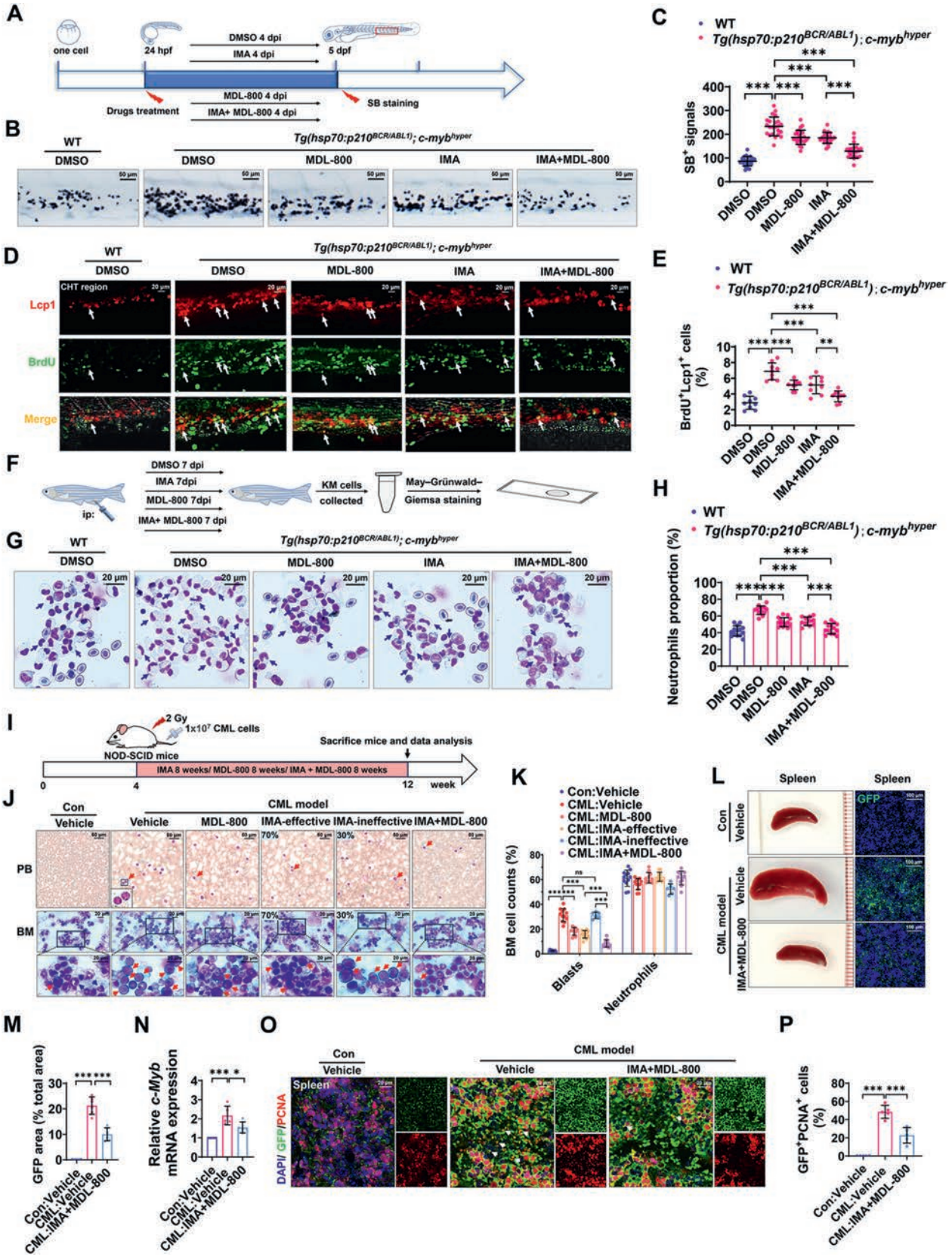

Figure 7 SIRT6 activator MDL-800 treatment with imatinib improves chemotherapy efficacy. (A) Flowchart of imatinib (IMA) or/and MDL-800 treatment in zebrafish embryos. (B) SB staining of the zebrafish larvae with IMA or/and MDL-800 treatment in the CHT region at 5 dpf. (C) Average numbers of SB^+ cells per embryo with drug treatment at 5 dpf ($n > 20$ embryos per group). (D) Double staining of myeloid cell marker Lcp1 and BrdU in the zebrafish larvae with or without drug treatment in the CHT region at 5 dpf. White arrows indicate $BrdU^+$ $Lcp1^+$ cells. (E)

non-responsiveness. Future studies with well-annotated human samples are crucial to validate the clinical utility of SIRT6 and c-MYB expression in guiding treatment decisions.

Notably, we established an endogenous *sirt6*-mutant zebrafish model that recapitulates key features of human MPN across developmental stages. This model provides a valuable *in vivo* platform for studying *sirt6*-deficient leukemogenesis, including its effects on genomic stability, telomere function, and metabolism. It is also well-suited for future genetic screens to uncover synergistic variants, and therapeutic targets. Mechanistic insights derived from this model will deepen our understanding of leukemogenesis and chemotherapy sensitivity.

We further elucidated a previously unreported mechanism wherein Sirt6 physically interacted with the *c-myb* promoter region and epigenetically represses its transcriptional activity through histone H3K9 deacetylation. Genome-wide profiling of SIRT6 binding revealed significant enrichment not only at the *c-MYB* promoter but also at promoters of other genes, including *WNT2b* and *MYC* (data not shown). Given previous studies linking aberrant *Wnt/β-catenin* activation has been linked to imatinib resistance in CML[9,66], the ability of SIRT6 activation to overcome resistance may extend beyond *c-MYB* suppression and involve downregulation of additional pro-survival pathways, such as *Wnt/β-catenin* signaling-an important avenue for future research.

The role of SIRT6 in leukemogenesis appears context-dependent and varies across leukemia subtypes. In contrast to the tumor-suppressive function of Sirt6 we describe in MPN models, prior work has proposed an oncogenic role for SIRT6 in AML, where its inactivation impairs DNA repair mechanisms and promotes aggressive disease progression[67]. Supporting this subtype-specific paradigm, our analysis of patient bone marrow samples showed that SIRT6 expression was significantly downregulated in CML but elevated in AML. Such duality is not unique to SIRT6, for instance, SIRT1, the most extensively studied sirtuin in hematologic malignancies, has been reported to aggravate AML and CLL[68,69] yet exert protective effects in myelodysplastic syndrome (MDS)[70]. We propose that the context-dependent role of SIRT6 in leukemia is dictated by its distinct functions and downstream targets. In AML, SIRT6 may maintain genomic stability *via* DNA repair pathways (*e.g.*, deacetylating DNA-PKcs/CtIP)[67], so its loss promotes aggressiveness. In MPN, however, SIRT6 primarily suppresses proliferation by epigenetically regulating *c-Myb*. Thus, whether SIRT6 acts in a pro- or anti-tumorigenic manner depends on the dominant survival mechanisms operating in each malignancy.

5. Conclusions

Our work establishes SIRT6 as an important epigenetic regulator that inhibits neutrophil proliferation in myeloid disorders by directly repressing *c-MYB* transcription through H3K9 deacetylation. Our findings highlight SIRT6-activating agents as a potential therapeutic strategy to suppress neutrophil hyperplasia and enhance chemosensitivity in leukemia.

Acknowledgments

This study was supported by the Special Project for Marine Economic Development of Department of Natural Resources of Guangdong Province (GDNRC[2024]25, China), the National Natural Science Foundation of China (82104271, 82473921), Provincial Medical Science Research Fund Project of Guangdong Province (A2025222), Guangzhou Science and Technology Bureau Basic Research Program (2025A04J3998, 2025A04J3699, China), Scientific Research Capacity Improvement Project of Guangzhou Medical University (02-410-2405111, China), the team project of "Subject Enrichment, Innovation and Quality Improvement" in Guangdong Pharmaceutical University (2024ZZ08, China). The authors would like to thank Professor Zhiping Liu (Jinan University); Jin Xu, Yiyue Zhang and Qiang Wang (South China University of Technology) for their helpful suggestions.

Author contributions

Luping Wang: Investigation, Writing-original draft, Visualization, Methodology, Formal analysis, Funding acquisition, Data curation. Xiaoqian Wu: Visualization, Formal analysis, Writing-review & editing. Panxia Wang: Investigation, Visualization, Data curation. Minshan Zhang: Investigation, Visualization. Li Li: Investigation, Visualization, Formal analysis. Zhenhan Huang: Investigation, Visualization. Yang Mao: Investigation, Visualization. Haoming Chen: Investigation. Qin Wen: Investigation. Wei Liu: Supervision, Resources, Conceptualization. Zhibin Huang: Supervision, Resources, Conceptualization. Feifei Li: Supervision, Conceptualization. Juan Shen: Writing-review & editing, Visualization, Supervision, Resources, Project administration, Funding acquisition, Conceptualization.

Conflicts of interest

The authors declare no conflicts of interest.

Appendix A. Supporting information

Supporting information to this article can be found online at https://doi.org/10.1016/j.apsb.2026.06.020.

Quantification for the percentage of $BrdU^+Lcp1^+$ cells in zebrafish larvae ($n = 9$ larvae per group). (F) Flowchart of IMA or/and MDL-800 treatment in adult zebrafish. (G) May−Grünwald−Giemsa staining of KM cells obtained from adult zebrafish with indicated drugs intraperitoneal injection (i.p). (H) The proportion of neutrophils was calculated ($n > 12$ adults per group). (I) Flowchart of IMA or/and MDL-800 treatment in K562-eGFP cell-derived xenograft NOD-SCID mouse leukemia model. (J) May−Grünwald−Giemsa staining of PB and BM blood cells obtained from mice with or without indicated drugs treatment. (K) The proportions of blasts and neutrophils were calculated (Con: Vehicle: $n = 12$; CML: Vehicle: $n = 12$; CML: MDL-800: $n = 11$; CML: IMA-efective: $n = 12$; CML: IMA-ineffective: $n = 6$; CML: IMA + MDL-800: $n = 11$). (L) Gross appearance of spleen, IF of spleen from mice with or without IMA + MDL-800 treatment. (M) The area percentage of $K562\text{-}GFP^+$ cells infiltration in the spleen ($n = 6$). (N) The mRNA expression of *c-Myb* from BM blood cells ($n = 5$). (O) Triple staining of DAPI, GFP and PCNA in the frozen sections of spleen (white arrows indicate GFP^+PCNA^+ cells). (P) The percentage of GFP^+PCNA^+ cells ($n = 5$). Data are presented as mean ± SD. ns: not significant, $^*P < 0.05$, $^{**}P < 0.01$, $^{***}P < 0.001$.

References

1. Savona MR, Malcovati L, Komrokji R, Tiu RV, Mughal TI, Orazi A, et al. An international consortium proposal of uniform response criteria for myelodysplastic/myeloproliferative neoplasms (MDS/MPN) in adults. *Blood* 2015;**125**:1857−65.
2. Gottesman MM, Robey RW, Ambudkar SV. New mechanisms of multidrug resistance: an introduction to the cancer drug resistance special collection. *Cancer Drug Resist* 2023;**6**:590−5.
3. Sharma V, Wright KL, Epling-Burnette PK, Reuther GW. Metabolic vulnerabilities and epigenetic dysregulation in myeloproliferative neoplasms. *Front Immunol* 2020;**11**:604142.
4. Vainchenker W, Kralovics R. Genetic basis and molecular pathophysiology of classical myeloproliferative neoplasms. *Blood* 2017;**129**:667−79.
5. Jin Y, Qi X, Yu X, Cheng X, Chen B, Wu M, et al. Discovery of a potential hematologic malignancies therapy: selective and potent HDAC7 PROTAC degrader targeting non-enzymatic function. *Acta Pharm Sin B* 2025;**15**:1659−79.
6. Xu L, Zhang Z, Yu J, Ji T, Cheng J, Fei X, et al. *USP20* as a super-enhancer-regulated gene drives T-ALL progression *via* HIF1A deubiquitination. *Acta Pharm Sin B* 2025;**15**:4751−71.
7. Zhang W, Wan H, Feng G, Qu J, Wang J, Jing Y, et al. SIRT6 deficiency results in developmental retardation cynomolgus monkeys. *Nature* 2018;**560**:661−5.
8. Xu X, Zhang Q, Wang X, Jin J, Wu C, Feng L, et al. Discovery of a potent and highly selective inhibitor of SIRT6 against pancreatic cancer metastasis *in vivo*. *Acta Pharm Sin B* 2024;**14**:1302−16.
9. Li J, Wang X, Ding J, Zhu Y, Min W, Kuang W, et al. Development and clinical advancement of small molecules for *ex vivo* expansion of hematopoietic stem cell. *Acta Pharm Sin B* 2022;**12**:2808−31.
10. Huang Y, Yuan T, Liu B, Liang R, Liu K, Chuang S. GCIP and SIRT6 cooperatively suppress ITGAV gene expression by modulating c-myc transcription ability. *J Biol Chem* 2025;**301**:108314.
11. Wu X, Liu H, Brooks A, Xu S, Luo J, Steiner R, et al. SIRT6 mitigates heart failure with preserved ejection fraction in diabetes. *Circ Res* 2022;**131**:926−43.
12. Wang H, Diao D, Shi Z, Zhu X, Gao Y, Gao S, et al. SIRT6 controls hematopoietic stem cell homeostasis through epigenetic regulation of Wnt signaling. *Cell Stem Cell* 2016;**18**:495−507.
13. Liu M, Liang K, Zhen J, Zhou M, Wang X, Wang Z, et al. Sirt6 deficiency exacerbates podocyte injury and proteinuria through targeting Notch signaling. *Nat Commun* 2017;**8**:413.
14. Zhong L, D'Urso A, Toiber D, Sebastian C, Henry RE, Vadysirisack DD, et al. The histone deacetylase Sirt6 regulates glucose homeostasis *via* Hif1α. *Cell* 2010;**140**:280−93.
15. van Galen P, Hovestadt V, Wadsworth II MH, Hughes TK, Griffin GK, Battaglia S, et al. Single-cell RNA-Seq reveals AML hierarchies relevant to disease progression and immunity. *Cell* 2019;**176**:1265−81.
16. Ciciro Y, Sala A. MYB oncoproteins: emerging players and potential therapeutic targets in human cancer. *Oncogenesis* 2021;**10**:19.
17. Anand S, Vikramdeo KS, Sudan SK, Sharma A, Acharya S, Khan MA, et al. From modulation of cellular plasticity to potentiation of therapeutic resistance: new and emerging roles of MYB transcription factors in human malignancies. *Cancer Metastasis Rev* 2024;**43**:409−21.
18. Biersack B, Hopfner M. Emerging role of MYB transcription factors in cancer drug resistance. *Cancer Res* 2024;**7**:15.
19. Kimmel CB, Ballard WW, Kimmel SR, Ullmann B, Schilling TF. Stages of embryonic development of the zebrafish. *Dev Dyn* 1995;**203**:253−310.
20. Sun J, Liu W, Li L, Chen J, Wu M, Zhang Y, et al. Suppression of Pu.1 function results in expanded myelopoiesis in zebrafish. *Leukemia* 2013;**27**:1913−7.
21. Xu M, Ye Y, Ye Za, Xu Se, Liu W, Xu J, et al. Human BCR/ABL1 induces chronic myeloid leukemia-like disease in zebrafish. *Haematologica* 2020;**105**:674−86.
22. Liu W, Wu M, Huang Z, Lian J, Chen J, Wang T, et al. c-myb hyperactivity leads to myeloid and lymphoid malignancies in zebrafish. *Leukemia* 2017;**31**:222−33.
23. Lin HF, Traver D, Zhu H, Dooley K, Paw BH, Zon LI, et al. Analysis of thrombocyte development in CD41-GFP transgenic zebrafish. *Blood* 2005;**106**:3803−10.
24. Hall C, Flores MV, Storm T, Crosier K, Crosier P. The zebrafish lysozyme C promoter drives myeloid-specific expression in transgenic fish. *BMC Dev Biol* 2007;**7**:42.
25. Le Guyader D, Redd MJ, Colucci-Guyon E, Murayama E, Kissa K, Briolat V, et al. Origins and unconventional behavior of neutrophils in developing zebrafish. *Blood* 2008;**111**:132−41.
26. Wang K, Huang Z, Zhao L, Liu W, Chen X, Meng P, et al. Large-scale forward genetic screening analysis of development of hematopoiesis in zebrafish. *J Genet Genomics* 2012;**39**:473−80.
27. Thisse C, Thisse B. High-resolution *in situ* hybridization to whole-mount zebrafish embryos. *Nat Protoc* 2008;**3**:59−69.
28. Traver D, Paw BH, Poss KD, Penberthy WT, Lin S, Zon LI. Transplantation and *in vivo* imaging of multilineage engraftment in zebrafish bloodless mutants. *Nat Immunol* 2003;**4**:1238−46.
29. Sun W, Wang M, Zhao J, Zhao S, Zhu W, Wu X, et al. Sulindac selectively induces autophagic apoptosis of GABAergic neurons and alters motor behaviour in zebrafish. *Nat Commun* 2023;**14**:5351.
30. Jin H, Li L, Xu J, Zhen F, Zhu L, Liu PP, et al. Runx1 regulates embryonic myeloid fate choice in zebrafish through a negative feedback loop inhibiting Pu.1 expression. *Blood* 2012;**119**:5239−49.
31. Jin H, Sood R, Xu J, Zhen F, English MA, Liu PP, et al. Definitive hematopoietic stem/progenitor cells manifest distinct differentiation output in the zebrafish VDA and PBI. *Development* 2009;**136**:647−54.
32. Soza-Ried C, Hess I, Netuschil N, Schorpp M, Boehm T. Essential role of *c-myb* in definitive hematopoiesis is evolutionarily conserved. *Proc Natl Acad Sci U S A* 2010;**107**:17304−8.
33. Kim D, Paggi JM, Park C, Bennett C, Salzberg SL. Graph-based genome alignment and genotyping with HISAT2 and HISAT-genotype. *Nat Biotechnol* 2019;**37**:907−15.
34. Liao Y, Smyth GK, Shi W. featureCounts: an efficient general purpose program for assigning sequence reads to genomic features. *Bioinformatics* 2014;**30**:923−30.
35. Love MI, Huber W, Anders S. Moderated estimation of fold change and dispersion for RNA-seq data with DESeq2. *Genome Biol* 2014;**15**:550.
36. Chen C, Chen H, Zhang Y, Thomas HR, Frank MH, He Y, et al. TBtools: an integrative toolkit developed for interactive analyses of big biological data. *Mol Plant* 2020;**13**:1194−202.
37. Leichsenring M, Maes J, Moessner R, Driever W, Onichtchouk D. Pou5f1 transcription factor controls zygotic gene activation in vertebrates. *Science* 2013;**341**:1005−9.
38. Furey TS. ChIP-seq and beyond: new and improved methodologies to detect and characterize protein-DNA interactions. *Nat Rev Genet* 2012;**13**:840−52.
39. Li H, Durbin R. Fast and accurate short read alignment with Burrows-Wheeler transform. *Bioinformatics* 2009;**25**:1754−60.
40. Ramirez F, Ryan DP, Gruening B, Bhardwaj V, Kilpert F, Richter AS, et al. deepTools2: a next generation web server for deep-sequencing data analysis. *Nucleic Acids Res* 2016;**44**:W160−5.
41. Yu G, Wang L, He Q. ChIPseeker: an R/Bioconductor package for ChIP peak annotation, comparison and visualization. *Bioinformatics* 2015;**31**:2382−3.
42. Guo Z, Li P, Ge J, Li H. SIRT6 in aging, metabolism, inflammation and cardiovascular diseases. *Aging Dis* 2022;**13**:1787−822.
43. Tennen RI, Berber E, Chua KF. Functional dissection of SIRT6: identification of domains that regulate histone deacetylase activity and chromatin localization. *Mech Ageing Dev* 2010;**131**:185−92.
44. Long D, Wu H, Tsang AW, Poole LB, Yoza BK, Wang X, et al. The oxidative state of cysteine thiol 144 regulates the SIRT6 glucose homeostat. *Sci Rep* 2017;**7**:11005.

45. Pan PW, Feldman JL, Devries MK, Dong A, Edwards AM, Denu JM. Structure and biochemical functions of SIRT6. *J Biol Chem* 2011;**286**: 14575−87.
46. Xu M, Xu H, Ling Y, Liu J, Song P, Fang Z, et al. Neutrophil extracellular traps-triggered hepatocellular senescence exacerbates lipotoxicity in non-alcoholic steatohepatitis. *J Adv Res* 2026;**79**:521−34.
47. Kirchberger S, Shoeb MR, Lazic D, Wenninger-Weinzierl A, Fischer K, Shaw LE, et al. Comparative transcriptomics coupled to developmental grading *via* transgenic zebrafish reporter strains identifies conserved features in neutrophil maturation. *Nat Commun* 2024;**15**:1792.
48. Hedrick CC, Malanchi I. Neutrophils in cancer: heterogeneous and multifaceted. *Nat Rev Immunol* 2022;**22**:173−87.
49. Michishita E, McCord RA, Berber E, Kioi M, Padilla-Nash H, Damian M, et al. SIRT6 is a histone H3 lysine 9 deacetylase that modulates telomeric chromatin. *Nature* 2008;**452**:492−6.
50. Toiber D, Erdel F, Bouazoune K, Silberman DM, Zhong L, Mulligan P, et al. SIRT6 recruits SNF2H to DNA break sites, preventing genomic instability through chromatin remodeling. *Mol Cell* 2013;**51**:454−68.
51. Liao X, Li F, Yu F, Ye L. Epigenetically rewiring metabolic genes *via* SIRT6 orchestrates MSC fate determination. *Stem Cell* 2024;**42**:821−9.
52. Gorre ME, Mohammed M, Ellwood K, Hsu N, Paquette R, Rao PN, et al. Clinical resistance to STI-571 cancer therapy caused by BCR-ABL gene mutation or amplification. *Science* 2001;**293**:876−80.
53. Hochhaus A, Larson RA, Guilhot F, Radich JP, Branford S, Hughes TP, et al. Long-term outcomes of imatinib treatment for chronic myeloid leukemia. *N Engl J Med* 2017;**376**:917−27.
54. Cohen P, Cross D, Janne PA. Kinase drug discovery 20 years after imatinib: progress and future directions. *Nat Rev Drug Discov* 2021; **20**:551−69.
55. Ye Y, Yang X, Li F, Liu W, Zhang W, Huang Z. c-myb is involved in CML progression and is a therapeutic target in the zebrafish CML model. *Animal Model Exp Med* 2024;**7**:136−44.
56. Rodrigues A, Gromicho M, Costa Gomes B, Rueff J. Methylation status of selected microRNAs in imatinib-sensitive and imatinib-resistant chronic myeloid leukaemia (K562) cell lines. *Eur J Cancer* 2013;**49**:S122.
57. Paul T, Roy R, Sarkar RD, Sinha S, Biswas N. H2O2 mediated FLIP and XIAP down-regulation involves increased ITCH expression and ERK−Akt crosstalk in imatinib resistant chronic myeloid leukemia cell line K562. *Free Radical Biol Med* 2021;**166**:265−76.
58. Zhang Y, Jin H, Li L, Qin FX, Wen Z. cMyb regulates hematopoietic stem/progenitor cell mobilization during zebrafish hematopoiesis. *Blood* 2011;**118**:4093−101.
59. Pattabiraman DR, Gonda TJ. Role and potential for therapeutic targeting of *MYB* in leukemia. *Leukemia* 2013;**27**:269−77.
60. Nason-Burchenal K, Wolff L. Activation of c-myb is an early bone-marrow event in a murine model for acute promonocytic leukemia. *Proc Natl Acad Sci U S A* 1993;**90**:1619−23.
61. Li X, Wang L, Qin X, Chen X, Li L, Huang Z, et al. Estrogens revert neutrophil hyperplasia by inhibiting Hif1α−cMyb pathway in zebrafish myelodysplastic syndromes models. *Cell Death Discov* 2022;**8**: 323.
62. Nepali K, Liou J. Recent developments in epigenetic cancer therapeutics: clinical advancement and emerging trends. *J Biomed Sci* 2021;**28**:27.
63. Peart MJ, Smyth GK, van Laar RK, Bowtell DD, Richon VM, Marks PA, et al. Identification and functional significance of genes regulated by structurally different histone deacetylase inhibitors. *Proc Natl Acad Sci U S A* 2005;**102**:3697−702.
64. An X, Tiwari AK, Sun Y, Ding P, Ashby CR Jr, Chen Z. BCR-ABL tyrosine kinase inhibitors in the treatment of Philadelphia chromosome positive chronic myeloid leukemia: a review. *Leuk Res* 2010;**34**: 1255−68.
65. Ross TS, Mgbemena VE. Re-evaluating the role of BCR/ABL in chronic myelogenous leukemia. *Mol Cell Oncol* 2014;**1**:e963450.
66. Nagao R, Ashihara E, Kimura S, Strovel JW, Yao H, Takeuchi M, et al. Growth inhibition of imatinib-resistant CML cells with the T315I mutation and hypoxia-adaptation by AV65—a novel Wnt/β-catenin signaling inhibitor. *Cancer Lett* 2011;**312**:91−100.
67. Cagnetta A, Soncini D, Orecchioni S, Talarico G, Minetto P, Guolo F, et al. Depletion of SIRT6 enzymatic activity increases acute myeloid leukemia cells' vulnerability to DNA-damaging agents. *Haematologica* 2018;**103**:80−90.
68. Sasca D, Haehnel PS, Szybinski J, Khawaja K, Kriege O, Pante SV, et al. SIRT1 prevents genotoxic stress-induced p53 activation in acute myeloid leukemia. *Blood* 2014;**124**:121−33.
69. Audrito V, Vaisitti T, Rossi D, Gottardi D, D'Arena G, Laurenti L, et al. Nicotinamide blocks proliferation and induces apoptosis of chronic lymphocytic leukemia cells through activation of the p53/miR-34a/SIRT1 tumor suppressor network. *Cancer Res* 2011;**71**: 4473−83.
70. Sun J, He X, Zhu Y, Ding Z, Dong H, Feng Y, et al. SIRT1 activation disrupts maintenance of myelodysplastic syndrome stem and progenitor cells by restoring TET2 function. *Cell Stem Cell* 2018;**23**: 355−69.